Titre: Title:	Phonon Transport Analysis of Thermal Conductivity in Particulate Nanocomposites
Auteur: Author:	Arash Behrang
Date:	2012
Type:	Mémoire ou thèse / Dissertation or Thesis
Référence: Citation:	Behrang, A. (2012). Phonon Transport Analysis of Thermal Conductivity in Particulate Nanocomposites [Mémoire de maîtrise, École Polytechnique de Montréal]. PolyPublie. https://publications.polymtl.ca/921/

URL de PolyPublie: PolyPublie URL:	https://publications.polymtl.ca/921/
Directeurs de recherche: Advisors:	Pierre Lafleur, Miroslav Grmela, & Charles Dubois
Programme: Program:	Génie chimique

UNIVERSITÉ DE MONTRÉAL

PHONON TRANSPORT ANALYSIS OF THERMAL CONDUCTIVITY IN PARTICULATE NANOCOMPOSITES

ARASH BEHRANG
DÉPARTEMENT DE GÉNIE CHIMIQUE
ÉCOLE POLYTECHNIQUE DE MONTRÉAL

MÉMOIRE PRÉSENTÉ EN VUE DE L'OBTENTION
DU DIPLÔME DE MAÎTRISE ÈS SCIENCES APPLIQUÉES
(GÉNIE CHIMIQUE)
AOÛT 2012

UNIVERSITÉ DE MONTRÉAL

ÉCOLE POLYTECHNIQUE DE MONTRÉAL

Ce mémoire intitulé:

PHONON TRANSPORT ANALYSIS OF THERMAL CONDUCTIVITY IN PARTICULATE NANOCOMPOSITES

présenté par: BEHRANG Arash
en vue de l'obtention du diplôme de: Maîtrise ès Sciences Appliquées
a été dûment accepté par le jury d'examen constitué de:

M. LEGROS Robert, Ph.D., président
M. LAFLEUR Pierre, Ph.D., membre et directeur de recherche
M. GRMELA Miroslav, Ph.D., membre et codirecteur de recherche
M. DUBOIS Charles, Ph.D., membre et codirecteur de recherche
M. FAVIS Basil, Ph.D., membre

Dedication

I dedicate this dissertation to my family. You are my life, my love and my reason for being. It is dedicated to my lovely wife, Sara with love. I am truly grateful for her immense love and patience throughout my graduate career. A special feeling of gratitude to my father and mother who have never left my side and supported me spiritually and materially since I was born.

Acknowledgement

First and foremost, I would like to express my unyielding gratitude to my supervisors, Professor Miroslav Grmela, Professor Charles Dubois and Professor Pierre Lafleur for their unselfish guidance, expertise, and friendship. They always took the time to guide me, to challenge me, and to help me develop my skills as a scientist and as a person.

Résumé

Les modèles théoriques ont été présentés pour la prédiction de la conductivité thermique de composites constitués de particules sphériques. Parmi ces modèles, seuls quelques-uns d'entre eux sont en mesure de prédire correctement la conductivité thermique de nanocomposites. La difficulté à modéliser correctement cette propriété physique origine de la différence entre la conductivité de la matrice et des particules à l'état pur par rapport à leurs valeurs respectives dans le composite. En conséquence, la résistance thermique à l'interface entre la matrice et les particules devient une variable importante de la conductivité thermique des matériaux nanocomposites. Dans ce projet, l'analyse de l'échange des phonons thermiques dans les milieux hétrogénes est réalisée et une formule générale de la conductivité thermique effective de nanocomposites est présentée.

Dans la premire étape du travail, le transport de phonons à l'interface entre la matrice et des nanoparticules est étudié. Cette investigation vise présenter la résistance thermique sous une nouvelle forme. Les deux types de transport de phonons sur l'interface particule-matrice, soient diffus et spéculaire, sont pris en compte dans le calcul de la conductivité thermique effective pour les nanocomposites particulaires.

Dans un deuxième temps, le modèle proposé est évalué en regard de résultats numériques et expérimentaux disponibles dans la littérature. Cette évaluation tend à prouver que le modèle proposé est capable de prédire la conductivité thermique effective pour un large éventail de fractions volumiques et de tailles de particules.

Abstract

Theoretical models have been presented for predicting the thermal conductivity of composites consisting of spherical particles. Among these models, only a few of them are able to predict the thermal conductivity of nanocomposites. This is because the matrix and particle thermal conductivities in nanocomposites are not equal to their bulk values due to increased interface scattering. The boundary scattering becomes important when the characteristic length of the media is smaller than the bulk mean free path of phonons. The thermal boundary resistance at the interface between matrix and suspended particles is affected on the thermal conductivity of nanocomposites. In this work, the phonon viewpoint of heat transport in heterogeneous media is investigated and a general formula for the effective thermal conductivity of particulate nanocomposites is presented.

In the first step of this project, the phonon scattering at the interface between matrix and nanoparticles is investigated. This study aims to present the thermal boundary resistance in a new form. Both diffuse and specular types of scattering of phonons on the particle-matrix interface are taken into account in the derivation of the effective thermal conductivity for the particulate nanocomposites.

In the next step, the proposed model is evaluated with numerical and experimental results available in literature. This evaluation is done to prove that the proposed model is able to predict the effective thermal conductivity in a wide range of the volume fractions and particle sizes.

Table of Contents

List of Tables

List of Figures

Chapter 1

Introduction

Introduction

Heat transfer in nano-scale differs significantly from that in the bulk material (macro-scale) since the characteristic length (i.e., diameter of wires and spherical particles and thickness of thin films) of the media is comparable to the mean free path of heat carriers. Three different types of heat carriers would be defined: phonons in semiconductors, electrons in conductors and photons in radiation heat transfer. In this condition, local thermal equilibrium assumption breaks down and, consequently, conventional Fourier heat conduction cannot be directly applied. Furthermore, the heat transport becomes ballistic rather than diffusive. For the ballistic regime, temperature jumps occur at the boundaries of the media.

Boltzmann transport equation is the most commonly used method to study the heat transfer of the nanostructures. Various techniques have been developed to solve the Boltzmann transport equation in different geometries and conditions in order to provide more precise results.

Particle size and shape, volume fraction, orientation and the thermal conductance at the interface between two dissimilar materials are affected by the thermal conductivity of the inhomogeneous systems. For a heterogeneous media, such as nanocomposites and supperlattices, interfacial effects are very important. Phonon scattering at the interface forms a resistance against the motion of phonons and, consequently, decreases the phonon mean free path. This reduction in the phonon mean free path finally leads to a reduction in the effective thermal conductivity. While this term (i.e., interfacial effects) would be neglected in macrostructures, when a heterogeneous media is under investigation, a better understanding of the behaviour of phonons at the interface between dissimilar materials is required. The interface can behave diffusely or specularly. Due to confinement of the phonon transport in the diffuse boundary scattering, the diffuse thermal conductivity is smaller than the specular thermal conductivity.

The main objective of this Master's project is to introduce a new model to study the effective thermal conductivity of an inhomogeneous (suspended spherical particles in matrix) media by including the additional analysis details of the complex physics involved in the phonon scattering on the particle-matrix interface. To meet this goal, the following specific objectives have been considered:

(i). Modeling the thermal conductivity of composite using the generalized self-consistent method.

(ii). Study the phonon transport at the interface between the matrix and particles and

present a new term for the thermal boundary resistance.

(*iii*). Study the effects of particle size, volume fraction of particles, and specular probability on the effective thermal conductivity of the nanocomposite and compare results with experimental data and previous numerical results.

In the scope of these specific objectives, by using the definition of the equilibrium thermal boundary resistance and the thermal conductivity based on the kinetic theory, the thermal boundary resistance is presented in the form of the mean free path. Then, both diffuse and specular types of phonon scattering on the particle-matrix interface are studied in the derivation of the totally diffuse, totally specular, and partially diffuse-partially specular thermal boundary resistance mean free paths. Finally, a generic model is introduced to study the thermal conductivity of the nanocomposite comprising spherical particles.

Chapter 2

Background

2.1 Heat Transfer

The energy transport process is a consequence of temperature difference known as heat transfer. Heat transfer phenomena are commonly seen in our everyday life and play a significant role in many industries and applications. Depending on the nature of the medium, three types of heat carriers are defined. Heat carriers convey heat from one side or arbitrary point to the other. Electrons, phonons, and photons are the most important heat carriers under different conditions. In a radiation mechanism, heat is carried by photons while in conductors and semiconductors, heat is carried by electrons and phonons, respectively. According to the principle of quantum mechanics, both the wave and particle natures of phonons would be studied in the heat transfer. The scattering among the phonons causes them to thermalize their energy and transfer heat from one point to another. Adequate scattering of the phonons establishes the local thermal equilibrium state where the temperature gradient can be defined [1, 2]. Although heat transfer is inherently a non-equilibrium concept, the local thermal equilibrium is established where the deviation from equilibrium state is negligible. It is remarked that the classic irreversible thermodynamics (CIT) provides sufficient concepts to describe the equilibrium state. The classic irreversible thermodynamics breaks down under non-equilibrium conditions where basic physical quantities, such as temperature and mass, are not the only function of place (size and time dependency become effective) [3, 4]. In the macro-scale, the thermal conductivity coefficient is defined as a ratio between the heat flux (q) and the temperature gradient (∇T) in the form of the well-known Fourier's law.

$$q = -k\nabla T \tag{2.1}$$

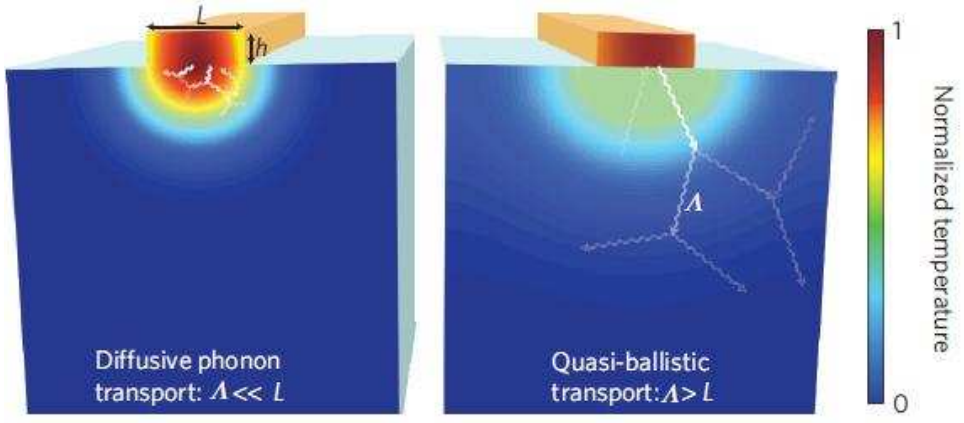

Figure 2.1: Schematic illustration of heat transfer under diffuse and ballistic regimes [2].

By k, we denote the thermal conductivity of the media. Fourier's law is a famous approach in the formulation of the macroscopic heat conduction, where the dependence of size and time on the heat transport is not important [5]. The diffuse collision (i.e., experiencing many collisions between phonons) and infinite heat propagation velocity are important features of the Fourier heat conduction. It is experimentally observed and physically supposed that even the smallest change in the temperature gradient is sensed after relaxation time. On the other hand, any temperature disturbance propagates at the finite velocity. In micro and nano-scales where time and size dependence are important, the validity of Fourier heat conduction is questioned. The qualitative behaviour of the thermal transport under diffuse and ballistic regimes has been illustrated in Figure (2.1).

2.2 Phonons

In crystalline solids, atoms are structured in periodical arrays known as lattice. Lattice vibrations contribute to thermal conductivity. In non-metal solids, heat is transferred by phonons. If two atoms in a solid body are far apart, an attractive force exists between the atoms, while the interaction force becomes repulsive (because of the overlap of electronic orbits in the atoms), if two atoms are close to each other. The minimum potential defines the equilibrium positions of the atoms where the repulsive and attractive forces balance each other. Atoms in a solid body vibrate about their equilibrium position. The vibration of each atom is constrained by its neighbouring atoms through the interatomic potential. A mass-spring system is a simplified picture of the interatomic interaction in crystalline solids. In such a system, the vibration of the atoms is not independent of each other and can cause the vibration of the whole system by creating a lattice wave in the system.

Clearly, the atoms near the hot side of the solid have larger vibrational amplitudes, which will be felt by atoms of the other side of the solid through the propagation and interaction of the lattice waves.

According to the principle of quantum mechanics, the energy of each lattice wave is discrete and must be a multiple of energy ($h\omega$), where h is the Planck's constant and ω is the frequency. The minimum energy of $h\omega$, a quantized lattice wave, is called phonon. At a specific frequency and wavelength, phonon is a wave that travels through the entire crystal. Phonons can be considered as particles as long as they are much smaller than the crystal size. In this condition, the mass-spring picture of the crystal can be replaced by a box of phonon particles with random movement in the phase space.

Phonon dispersion curves are used to approximate how phonons are affected by the thermal conductivity of the media [4]. The phonon dispersion curves are usually divided into acoustic and optical branches. Low frequency acoustic phonon contributes significantly to thermal conductivity due to its large mean free paths. Although the optical phonon often does not contribute to heat transfer due to its small mean free path, it could be important when the characteristic length of the media is reduced [6–8].

2.3 Phonon Dispersion

The heat transfer in a solid is due to lattice vibration. This vibration is called thermal motion. Based on the lattice vibration theory, the atoms in a solid are close to each other, and interatomic forces keep them in position [9]. Vibration of the atoms takes place near their equilibrium positions. Understanding the interatomic forces enables us to further understand thermal properties of solids. If the bonds between two atoms are supposed to be stiff (such as, a rod), it will be impossible to determine the specific heat, thermal conductivity and melting point of the solid. Therefore, the elastic vibration model of the ball and spring should be considered (see Figure (2.2)). The spring is a conceptual representative of the repulsive and attractive forces [4, 10].

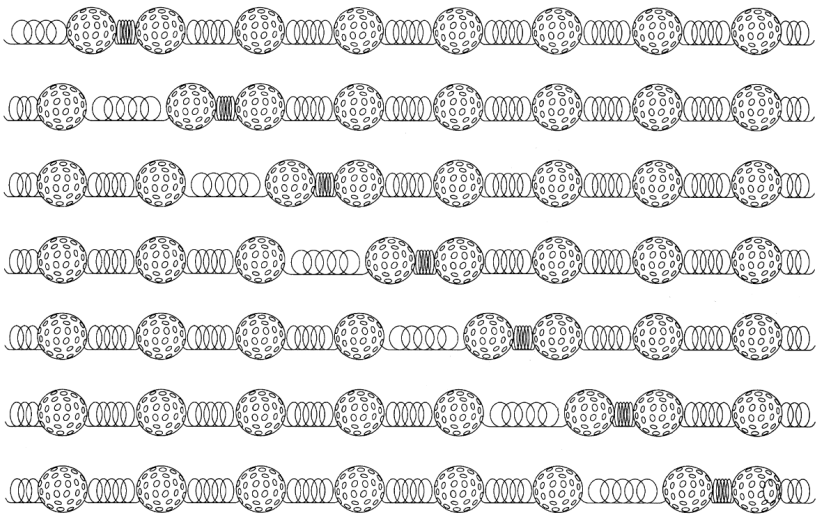

Figure 2.2: Ball-spring model for introducing of the speed of phonon propagation [10].

2.3.1 The vibration of crystal with a mono-atomic basis

It is assumed that the elastic response of crystal is a linear function of the force. So, Hook's law could be used. According to this assumption, a harmonic vibration between atoms is considered, while anharmonic vibration is discussed at higher temperatures. Another assumption in the lattice vibration is that forces on an atom only come from its nearest-neighbours. A mono-atomic chain is illustrated in Figure (2.3). Allowing all atom masses (M) and spring constants (C) to be the same, the equation of motion of the atoms could be written as follows:

$$F = -C(u_{s+1} - u_s) - C(u_s - u_{s-1}) \tag{2.2}$$

the equation of motion would be rearranged as follows:

$$M\frac{d^2u_s}{dt^2} = C(u_{s+1} - 2u_s + u_{s-1}) \tag{2.3}$$

The above equation is a special form of the differential wave equation

$$M\frac{d^2u_s}{dt^2} = Ca^2\frac{d^2u_s}{dx^2} \tag{2.4}$$

with a solution of the form $u_s = u\exp[-(i\omega t - kas)]$. Where ω is the frequency of vibration, k is the wave-vector, a is the spacing between the planes, and t is time [4].

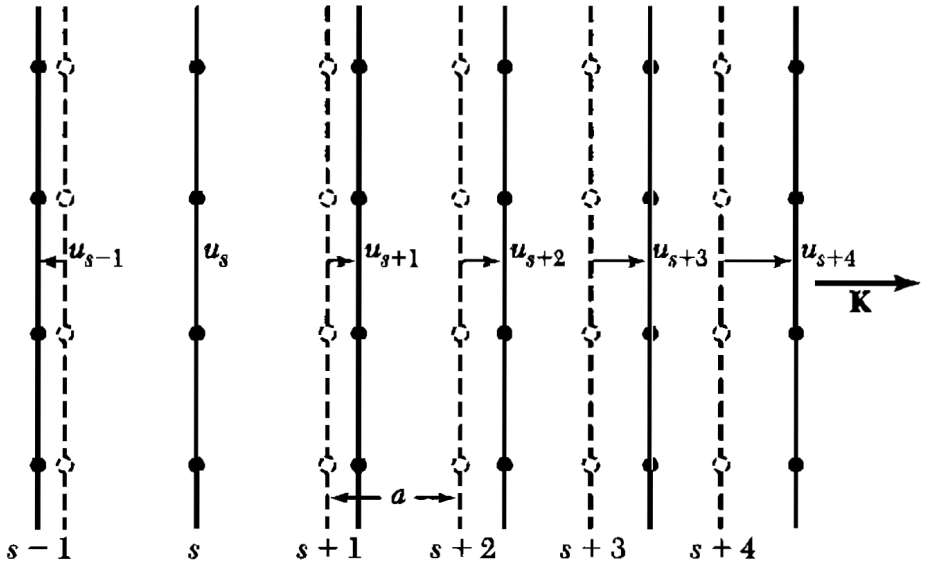

Figure 2.3: Mono-atomic vibration of an atom chain [9].

Displacements at $s \pm 1$ are

$$u_{s\pm1} = u \exp[-(i\omega t - ka(s \pm 1))] \tag{2.5}$$

Substituting the guessed expressions for u_s and $u_{s\pm1}$ into the equation (2.3) and after some manipulations, the frequency of vibration in the mono-atomic chain is

$$\omega = 2(\sqrt{\frac{C}{M}})|\sin(\frac{ak}{2})| \tag{2.6}$$

2.3.2 First Brillouin zone

Only the wave-vectors, which are in the first Brillouin zone are physically affected by elastic waves. At the boundaries of the first Brillouin zone, the group velocity of phonons ($v_g \equiv \partial\omega/\partial k$) is equal to zero, since the atoms at the boundaries oscillate in opposite directions and their average movement tends to zero [9]. The first Brillouin zone takes place between $-\pi/a < k < \pi/a$. The group velocity in the first Brillioun zone is

$$v_g = (\sqrt{\frac{Ca^2}{M}})\cos(\frac{ak}{2}) \tag{2.7}$$

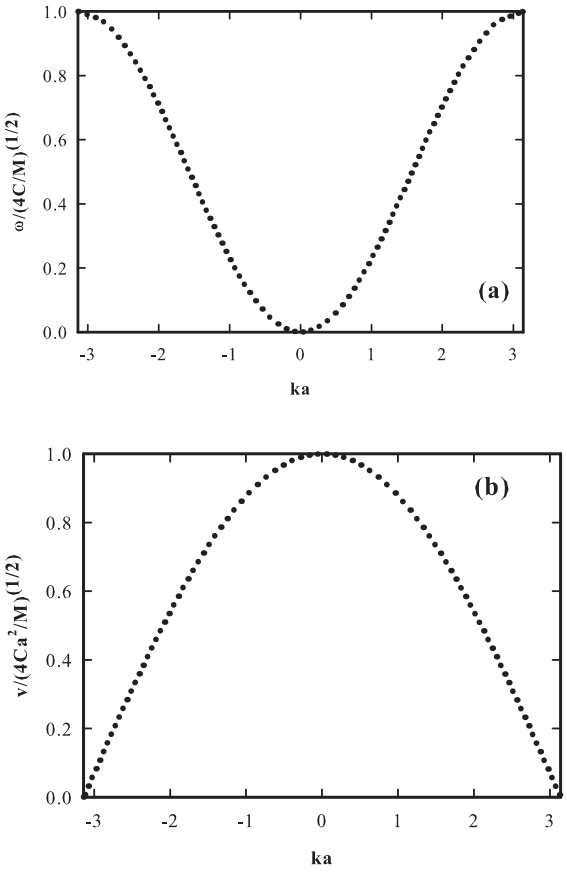

Figure 2.4: (a)Phonon dispersion curve of a one-dimensional mono-atomic lattice chain, (b)Group velocity of a one-dimensional mono-atomic lattice chain.

Phonon dispersion and phonon group velocity curves for a 1-D mono-atomic lattice chain are illustrated in Figure (2.4). As previously explained and schematically illustrated in (2.4), the group velocity of phonons is equal to zero when phonons are at the boundaries of the first Brillouin zone.

2.3.3 The vibration of crystal with a diatomic basis

The relationship between the vibration frequency and the phonon wave-vector for a di-atomic chain follows the same procedure as the mono-atomic one. The interatomic forces and the mass of the nearest-neighbour atoms are, however, not the same (Figure (2.5)). Equations of motion of the atoms are written as follows:

$$M_1 \frac{d^2 u_s}{dt^2} = -C_1(v_s - u_s) + C_2(u_s - v_{s-1}) \tag{2.8}$$

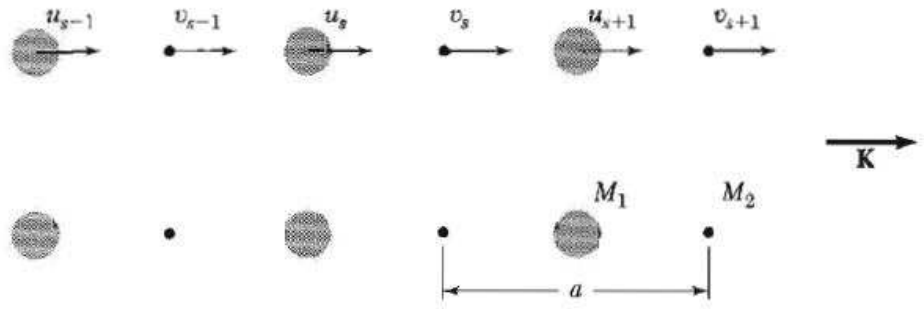

Figure 2.5: A chain of two atoms with different masses linked by springs with different constants [9].

$$M_2 \frac{d^2 v_s}{dt^2} = -C_2(u_{s+1} - v_s) + C_1(v_s - u_s) \tag{2.9}$$

Again, a wave form solution is guessed for the above equations. After some manipulations, we obtained the following equations:

$$(C_1 + C_2 - M_1\omega^2)u - (C_1 + C_2 \exp(iak))v = 0 \tag{2.10}$$

$$(C_1 + C_2 - M_2\omega^2)v - (C_1 + C_2 \exp(iak))u = 0 \tag{2.11}$$

The determinant must be zero,

$$2C_1C_2 - (C_1 + C_2)(M_1 + M_2)\omega^2 + M_1M_2\omega^4 - 2C_1C_2\cos(ak) = 0 \tag{2.12}$$

Solving the above equation, the phonon dispersion curve is represented for a diatomic chain. We use an example to introduce the phonon dispersion of a diatomic chain. Consider a linear diatomic chain in which the force constants are $C_1 = 10C$ and $C_2 = C$ with masses $M_1 = 10M$ and $M_2 = M$.

The result of the phonon dispersion curve when masses are not the same has been shown in Figure (2.6). Two branches are formed under this condition. The upper branch contains atoms, which oscillate out of phase. This branch is called the optical branch. The lower branch that corresponds to the in phase oscillation of atoms is called the acoustic branch [11]. The result of the group velocities of the acoustic and optical branches has been illustrated in Figure (2.6-b). The group velocity of the optical branch is significantly lower than the acoustic one. Note that the contribution of the optical branch in heat transfer can be neglected compared with the acoustic branch.

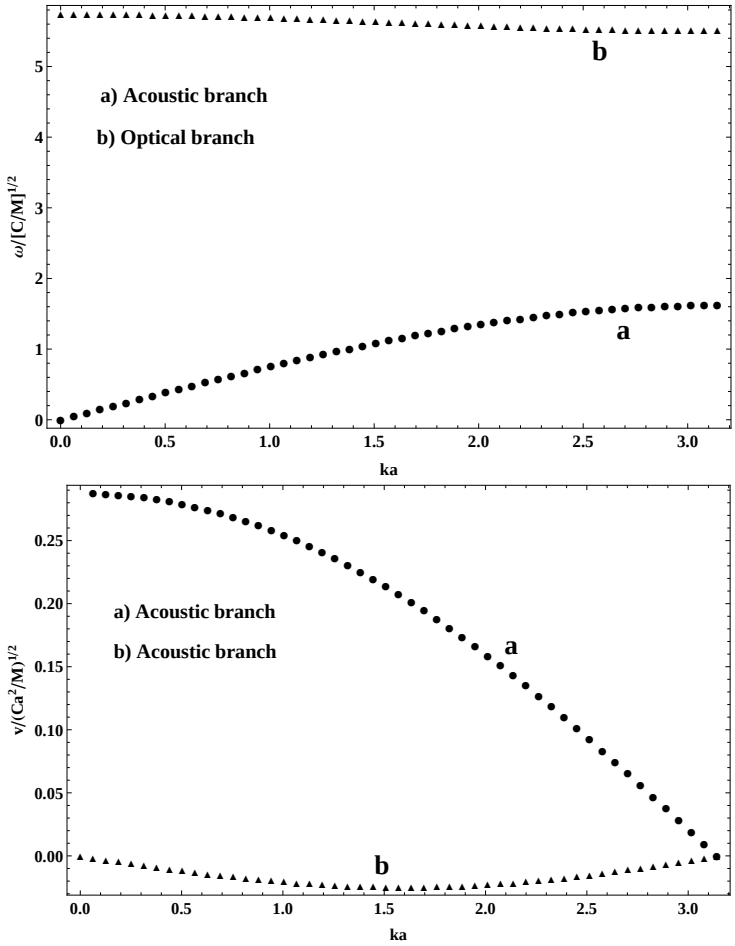

Figure 2.6: (a)Phonon dispersion curve of a one-dimensional diatomic lattice chain, (b)Group velocity of a one-dimensional diatomic lattice chain.

2.4 Macro and micro heat conduction

In heat conduction two major areas are studied; macro-scale and micro-scale. The characteristic times and lengths are used to differentiate these regimes from each other. As previously discussed, the local thermal equilibrium is applied to study the heat conduction under macro-scale assumption where the heat transfer is independent of time and size. While time and size dependence of the heat transport is considered in the micro-scale formulation. The spatial and temporal dependence of the heat transport leads to the definition of several parameters that are used in the characterization of the micro-scale heat transfer [4, 5].

A famous dimensionless number which is widely used in the study of heat transfer is called the Knudsen number ($Kn = \Lambda/L$). When the mean free path (Λ) of the heat carriers

(i.e., phonons in our work) is much less than the characteristic length (L) of the system, the heat transport occurs in the macroscopic state and the regime behaves in a purely diffuse manner. In the opposite case, the microscopic heat transfer is established when the mean free path is larger than the characteristic length of the system. In this condition, the micro-scale heat transfer is categorized into partially ballistic (ballistic-diffusive) or purely ballistic heat transfer [12]. Heat transfer based on the Knudsen number has been tabulated in Table (2.1).

Table 2.1: Heat transfer based on Knudsen number [11].

Regime	Method of calculation	Kn range
Continuum	Navir-Stokes and energy equation with no slip/jump boundary condition	$0.001 < Kn$
Slip flow	Navir-Stokes and energy equation with slip/jump boundary condition , DSMC	$0.001 < Kn < 0.1$
Transition	BTE, DSMC	$0 < Kn < 10$
(Free Molecule)		$Kn > 10$

2.4.1 Mean Free Path

Fourier's law is no longer valid when the characteristic length of the system is comparable or smaller than the mechanistic length, such as the mean free path. In order to better understand micro-scale heat transfer, the concept of the mean free path is described. The mean free path is the average distance covered by a moving particle (i.e., phonon in this work) between two subsequent collisions, which is affected by the direction and energy of the particle. The mean free path is usually used to estimate whether a phenomenon belongs to macro-scale regime or falls in the micro-scale regime [11, 13]. The chance of a successful collision between phonons decreases dramatically when the heat transfer regime falls into the micro-scale condition. On the other hand, the boundary scattering becomes significant and local thermal equilibrium is not valid unless it is at the boundaries [4].

2.4.2 Scattering mechanisms

The thermal conductivity of the media when $Kn >> 1$ decreases due to some scattering mechanism, which is not important in the corresponding bulk. Depending on the different types of scattering mechanisms, heat transfer is faced with different types of resistances shown in Figure (2.7). It is difficult to draw a conclusion about the relative strength of the scattering mechanisms on the thermal conductivity in the micro-scale media. It is

noted that phonon-boundary scattering is important in comparison with other scattering mechanisms, especially at low temperatures [6, 7, 14].

In addition to different scattering mechanisms exhibited in Figure (2.7), phonon-phonon collision also contributes to the heat transfer of the dielectric and semiconductor materials. There are two types of the phonon-phonon collisions called Umklapp (U-process) and normal (N-Process) processes. The N-process does not change the direction of the heat flux (both the energy and momentum are conserved), hence, the N-process does not contribute to thermal resistance. Phonon momentum is not conserved during the U-process, which creates resistance against heat flow and thus reduces the thermal conductivity of the media. It is noted that an infinite thermal conductivity is predicted, if the N-process is only taken into account [4, 11].

According to the Wien's displacement law for phonons, the phonon wavelength de-

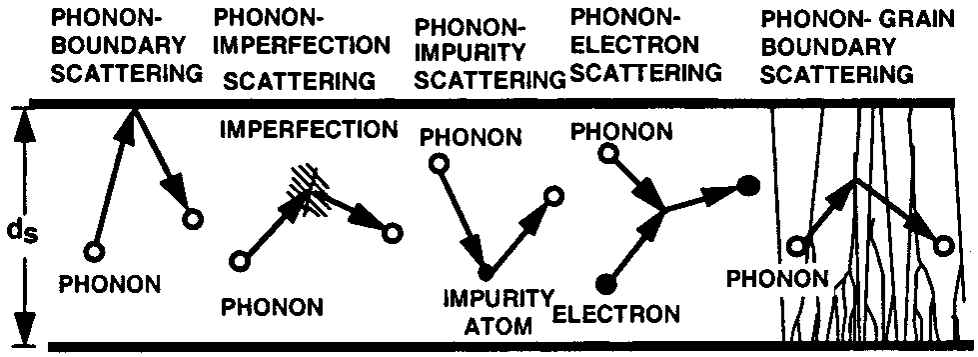

Figure 2.7: Different phonon scattering mechanisms that reduce the thermal conductivity of the medium [14].

pends inversely on temperature. Therefore, the wavelength of the dominant phonons significantly decreases as the temperature rises. Figure (2.8) is a plot of the thermal conductivity of $CoSb_3$ as a function of temperature. At low temperatures, the phonon wavelength is long and the Umklapp scattering does not make a significant contribution to the thermal conductivity. As the temperature gradually increases, the phonon wavelength obviously decreases and becomes comparable to the size of the defects. Thus, defect scattering becomes important in moderate temperatures. Consequently, at high temperatures, the phonon wavelength is shortened and the Umklapp scattering becomes important [8, 11].

In order to study both micro- and macro-scale heat transfers, the powerful Boltzmann transport equation is generally used.

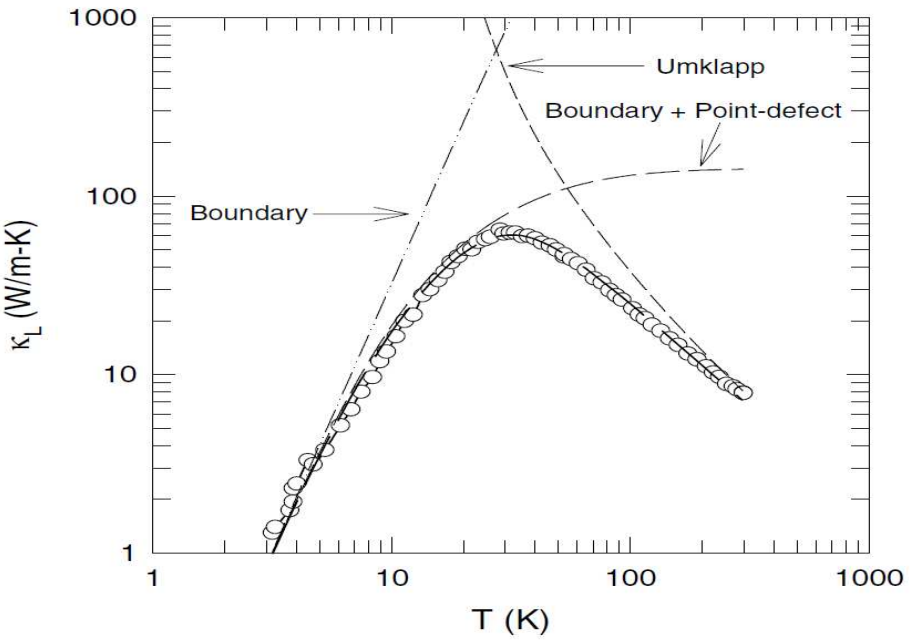

Figure 2.8: Thermal conductivity of $CoSb_3$ as a function of temperature. The dots and solid lines represent the experimental and theoretical results [8].

2.5 Boltzmann Transport Equation

Most transport theories in solids are derived based on the Boltzmann transport equation. The Boltzmann transport equation is applied to model both phonon and electron transport. Although phonons are inherently wave, the particle nature of phonons is considered when the characteristic length of the media is greater than the dominant phonon wavelength. Several types of heat conduction models are built upon the Boltzmann transport equation. Each model has tried to explain the thermal conductivity under different conditions and assumptions due to better coincidence with experimental results [6,7,12,15–18]. The Boltzmann transport equation gives us particle distribution in phase space at any time. It is used to study deviation from the equilibrium state when the temperature gradient is applied. The phonon distribution function ($f(r, v, t)$) gives the particle (number) density of phonons in the phase state at any given time. Suppose a particle at the spatial location r moves with a group velocity v at time t. At $t + dt$, without a collision, the particle will reach position $r + dr = r + vdt$ and its velocity will be $v + dv = v + adt$. Where a is the acceleration in a body force field [11]. Therefore

$$\frac{f(r + dr, v + dv, t + dt) - f(r, v, t)}{dt} = \frac{\partial f}{\partial t} + v.\frac{\partial f}{\partial r} + a.\frac{\partial f}{\partial v} = 0 \qquad (2.13)$$

The velocity of phonons in a dielectric material is fairly constant over a large range of frequencies, thus the third term of equation (2.13) can be neglected [5]. In the presence of the collision term, the Boltzmann transport equation can be written as

$$\frac{\partial f}{\partial t} + v.\frac{\partial f}{\partial r} = [\frac{\partial f}{\partial t}]_{coll} \tag{2.14}$$

The left hand side terms of the equation (2.14) describe the time evolution of the distribution function and convective transport of the distribution function due to the group velocity of the carriers. The term on the right hand side of the Boltzmann transport equation represents the scattering term, which brings the system back to the equilibrium state. The local equilibrium approximation is established when phonons collide with phonons, boundaries, defects, etc. In the ballistic heat conduction (i.e $Kn >> 1$), phonons are only scattered at the boundaries of the system and the local equilibrium assumption is valid only at the boundaries [19]. Since the Boltzmann transport equation is a nonlinear integro-differential equation, it cannot be exactly solved. The relaxation time approximation is often used in order to solve the Boltzmann transport equation. The relaxation time approximation assumes that the phonons slightly perturb the equilibrium state. Therefore

$$[\frac{\partial f}{\partial t}]_{coll} = \frac{f_0 - f}{\tau} \tag{2.15}$$

where f_0 is the equilibrium distribution, which is defined by Bose-Einstein distribution for phonons. By τ, we denote the relaxation time, which shows the deviation from the equilibrium state [4,7]. Several important heat conduction models based on the Boltzmann transport equation are derived in the next section.

2.5.1 Fourier's law

Fourier's law is widely and successfully used in the usual heat conduction problem where the characteristic length of the media is much greater than the mean free path of the energy carriers [12]. When the deviation from the equilibrium state is small, the local thermal equilibrium (LTE) is applicable. Enough scattering between phonons due to their energy being thermalized causes the local thermal equilibrium to be established. If the characteristic length of the system is assumed to be smaller than the mean free path, the local thermal equilibrium breaks down and the temperature cannot be defined in the conventional sense. The temperature jump due to the non-equilibrium nature of the phonon occurs under this condition. However, the media can be purely ballistic or

ballistic-diffusive [3]. These limits can be observed in Figure (2.9).

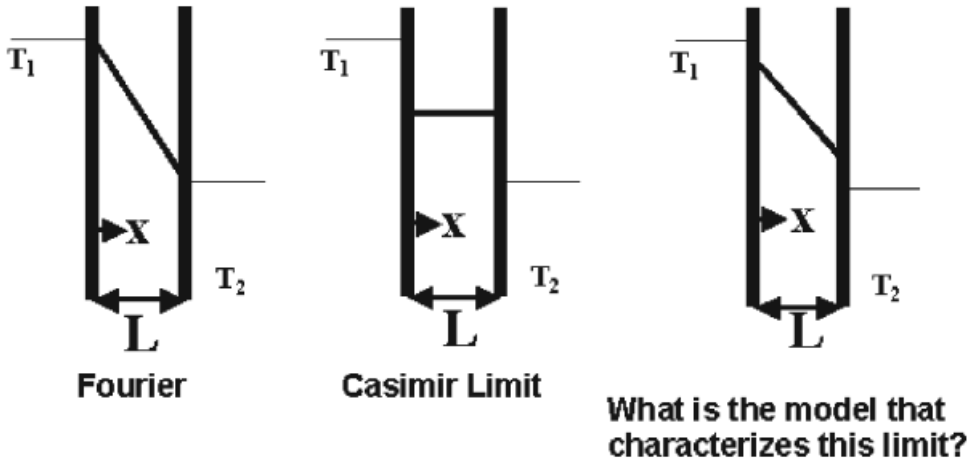

Figure 2.9: Schematic diagram qualitatively showing the temperature profiles under diffusive and ballistic phonon transport in steady sate condition [5].

Consider a phonon as a particle with energy $\hbar\omega$ and momentum $\hbar v$, when the characteristic length of the system is larger than the phonon wavelength. In this condition, the particle nature of the phonon could be considered. The internal energy is determined by multiplying $\hbar\omega$ by the number (density) of states $D(\omega)$, and the distribution function of phonons f, and integrating it over the phase space for a large range of frequencies. The internal energy for r-direction $(1-D)$ is given by

$$e = \int_0^{\omega_D} f(r)\hbar\omega D(\omega) d\omega \tag{2.16}$$

Consequently, the heat flux is obtained by multiplying the above equation by the group velocity of the phonon.

$$q_r = \int_0^{\omega_D} f(r)\hbar\omega D(\omega) v_r d\omega \tag{2.17}$$

Where ω_D is the Debye frequency. $\hbar$, ω and $D(\omega)$ are modified Plank's constant, frequency, and the density of states, respectively [11]. For a steady state condition, in a one dimensional case and under relaxation time approximation, the Boltzmann transport equation describes the diffusion of the particles and is written as follows [20]

$$v_r \frac{\partial f}{\partial r} = \frac{f_0 - f}{\tau} \tag{2.18}$$

under local thermal equilibrium conditions, we have

$$\frac{\partial f}{\partial r} = \frac{\partial f_0}{\partial r} = \frac{df_0}{dT}\frac{dT}{dr} \tag{2.19}$$

It is important that the local thermal equilibrium is applied in the presence of the temperature gradient. Substituting equation (2.19) in equation (2.18) leads to following expression

$$v_r \frac{df_0}{dT}\frac{dT}{dr} = \frac{f_0 - f}{\tau} \tag{2.20}$$

Rearranging the above equation

$$f - f_0 = -v_r \tau \frac{df_0}{dT}\frac{dT}{dr} \tag{2.21}$$

Multiplying equation (2.21) by $\hbar\omega D(\omega)v_r$ and integrating it over all frequencies gives

$$q_r = \int_0^{\omega_D} -v_r^2 \tau \hbar\omega D(\omega)\frac{df_0}{dT}\frac{dT}{dr}d\omega \tag{2.22}$$

Note that $\int_0^{\omega_D} f_0 \hbar\omega D(\omega)v_r d\omega = 0$. Because f_0 is equilibrium distribution.
The velocity of phonons is assumed to be identical in all directions ($v_r^2 = 1/3v^2$) and $\tau.v \equiv \Lambda$. By Λ, we denote the mean free path of the phonons. Thus, equation (2.22) is rewritten in the following form

$$q = -\frac{1}{3}\frac{dT}{dr} v\Lambda \int_0^{\omega_D} \frac{df_0}{dT}\hbar\omega D(\omega)d\omega \tag{2.23}$$

where $\int_0^{\omega_D} \frac{df_0}{dT}\hbar\omega D(\omega)d\omega$ is the internal energy with respect to temperature, which is known as the lattice specific heat C. Recalling equation (2.23) in the spirit of the lattice specific heat, we have

$$q = -\frac{1}{3} C v \Lambda \frac{dT}{dr} \tag{2.24}$$

where phonon thermal conductivity, k is $\frac{1}{3}Cv\Lambda$. Fourier's law is not able to predict the thermal conductivity of the media when the Knudsen number is comparable or larger than the unit. Note that an infinite speed of heat propagation (exerted heat flux is instantaneously sensed at every region of the media) is assumed by Fourier's law, which is not realistic [4, 11].

2.5.2 Hyperbolic heat equation (Cattaneo equation)

To overcome the prediction of the infinite speed of heat propagation, the Cattaneo equation was proposed. Although the Cattaneo equation can solve the drawback of Fourier's law for a characteristic time smaller than the relaxation time of the system, the validity of the Cattaneo equation for larger Knudsen numbers is still questioned [5, 13]. The unidirectional transient Boltzmann transport equation under relaxation time approximation is written as follows:

$$\frac{\partial f}{\partial t} + v_r \frac{\partial f}{\partial r} = \frac{f_0 - f}{\tau} \tag{2.25}$$

Multiplying equation (2.25) by $\hbar\omega D(\omega) v_r d\omega$ under the local thermal equilibrium approximation, we have

$$\int_0^{\omega_D} v_r \frac{df}{dt} \hbar\omega D(\omega) d\omega + \int_0^{\omega_D} v_r^2 \frac{df_0}{dT} \frac{dT}{dr} \hbar\omega D(\omega) d\omega = -\int_0^{\omega_D} \frac{f}{\tau} \hbar\omega D(\omega) v_r d\omega \tag{2.26}$$

After some manipulations

$$\tau \frac{dq}{dt} + q = -k \frac{dT}{dr} \tag{2.27}$$

The Cattaneo equation changes to Fourier's law for the steady state condition or $\tau = 0$. $\tau = 0$ corresponds to $c_w \to \infty$, implying thermal waves propagate at infinite speed. Note that $\tau = \frac{\alpha}{c_w^2}$, where c_w is thermal wave speed and α is the thermal diffusivity ($\alpha = \frac{k}{C}$). C is the volumetric specific heat capacity [11, 21].

2.5.3 Comparison between Fourier's law and Cattaneo equation

In order to compare Fourier's law and the Cattaneo equation, we consider a one-dimensional transient heat conduction problem across the thin film. The desirable film with a thickness of L is initially maintained at temperature T_0. At time $t = 0$, the temperature at $r = 0$ rises and reaches T_1, while the temperature at $r = L$ remains at T_0. This geometry has been widely used in several studies [12, 15, 22]. The following initial and boundary conditions are determined:

$$T(r,t)|_{r=0} = T_1 \tag{2.28}$$

$$T(r,t)|_{r=L} = T_0 \tag{2.29}$$

$$T(r,t)|_{t=0} = T_0 \tag{2.30}$$

Fourier's law is a well-known model for studying heat transport in macro-scale and steady state conditions, where the mean free path is smaller than the characteristic length (i.e., the film thickness). Fourier's law and the energy balance equation in a one-dimensional geometry are written as follows:

$$q = -k\frac{\partial T}{\partial r} \tag{2.31}$$

$$\frac{\partial u}{\partial t} = -\frac{\partial q}{\partial r} \tag{2.32}$$

where $\frac{\partial u}{\partial t}$ is the rate of change in internal energy, which can be defined as

$$\frac{\partial u}{\partial t} = C\frac{\partial T}{\partial t} \tag{2.33}$$

The divergence of equation (2.31) is substituted into equation (2.32) and the combination of them with equation (2.33), finally gives

$$\frac{\partial T}{\partial t} = \alpha\frac{\partial^2 T}{\partial r^2} \tag{2.34}$$

where α is thermal diffusivity defined as k/C. Equation (2.34) is used to present the temperature profile in the thin film. The following dimensionless variables are defined.

$$\theta = \frac{T - T_0}{T_1 - T_0} \tag{2.35}$$

$$\varsigma = \frac{r}{L} \tag{2.36}$$

$$\eta = \frac{t}{\tau} \tag{2.37}$$

Equation (2.34), initial and boundary conditions are rewritten in dimensionless forms as follows:

$$\frac{\partial \theta}{\partial \eta} = \Upsilon^2\frac{\partial^2 \theta}{\partial \varsigma^2} \tag{2.38}$$

$$\theta(\varsigma, \eta)|_{\varsigma=0} = 1 \tag{2.39}$$

$$\theta(\varsigma, \eta)|_{\varsigma=1} = 0 \tag{2.40}$$

$$\theta(\varsigma, \eta)|_{\eta=0} = 0 \tag{2.41}$$

Υ is equal to $\alpha\tau/L^2$. Equation (2.38) is a non-homogeneous partial differential equation. The non-homogeneous case is initially transformed into a homogeneous problem. A new

function, such as $\theta(\varsigma,\eta)=\omega(\varsigma,\eta)+\iota(\varsigma)$, is defined with one condition $\frac{\partial^2\iota}{\partial\varsigma^2}=\frac{\partial\iota}{\partial\eta}=0$. It is obvious that $\iota(\varsigma)$ is a linear function of ς and independent of η. After determining $\iota(\varsigma)$, equation (2.38) is finally described based on $\omega(\varsigma,\eta)$ instead of $\theta(\varsigma,\eta)$ in the homogeneous form with new boundary and initial conditions.

$$\frac{\partial\omega}{\partial\eta}=\Upsilon^2\frac{\partial^2\omega}{\partial\varsigma^2} \tag{2.42}$$

$$\omega(\varsigma,\eta)|_{\varsigma=0}=0 \tag{2.43}$$

$$\omega(\varsigma,\eta)|_{\varsigma=1}=0 \tag{2.44}$$

$$\omega(\varsigma,\eta)|_{\eta=0}=\varsigma-1 \tag{2.45}$$

The separation of variables method is used to solve the above-mentioned homogeneous partial differential equation and the non-dimensionless temperature profile is obtained as follows:

$$\theta(\varsigma,\eta)=1-\varsigma-\frac{2}{\pi}\sum_{n}^{\infty}\frac{\sin(n\pi\varsigma)}{n}\exp(-n^2\pi^2\Upsilon^2\eta) \tag{2.46}$$

To take into account the finite propagation of heat in the medium, Fouriers law should be modified [11]. The Cattaneo equation is an earlier attempt to predict the finite speed of heat propagation (see equation (2.27)). The divergence of equation (2.27) and time derivative of equation (2.32) give two equations, which are combined with equation (2.33) and give two equations to eliminate the heat flux term. Eliminating heat flux terms leads to the following differential equation:

$$\frac{\partial T}{\partial t}+\tau\frac{\partial^2 T}{\partial t^2}=\alpha\frac{\partial^2 T}{\partial r^2} \tag{2.47}$$

The same procedure as Fourier's law is applied to find the temperature profile equation. This system also is non-homogeneous under boundary conditions. Using dimensionless variables (equation (2.35)) and transferring the non-homogeneous system to homogeneous conditions, we have

$$\frac{\partial\omega}{\partial\eta}+\frac{\partial^2\omega}{\partial\eta^2}=\Upsilon^2\frac{\partial^2\omega}{\partial\varsigma^2} \tag{2.48}$$

$$\omega(\varsigma,\eta)|_{\varsigma=0}=0 \tag{2.49}$$

$$\omega(\varsigma,\eta)|_{\varsigma=1}=0 \tag{2.50}$$

$$\omega(\varsigma,\eta)|_{\eta=0}=\varsigma-1 \tag{2.51}$$

$$\frac{\partial\omega(\varsigma,\eta)|_{\partial\eta=0}}{\eta}=0 \tag{2.52}$$

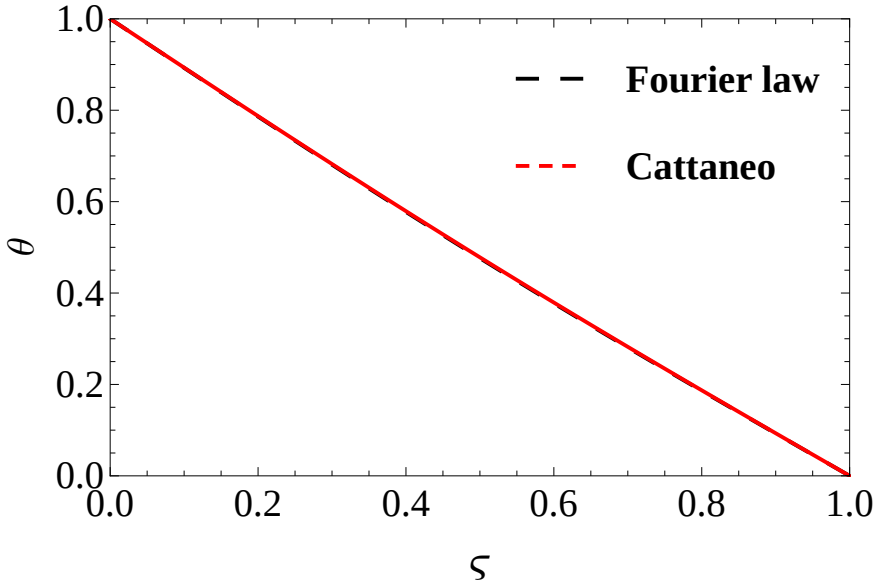

Figure 2.10: Temperature profile at the steady state condition in macroscopic domain.

Again, the separation of variables method is applied to achieve temperature profile.

$$\theta(\varsigma,\eta) = 1 - \varsigma - \frac{2}{\pi}\sum_{n}^{\infty} \exp^{\frac{-\eta}{2}}(\Psi\cos\frac{\eta\Psi}{2} + \sin\frac{\eta\Psi}{2})\frac{\sin(n\pi\varsigma)}{n\Psi} \tag{2.53}$$

where Ψ is related to $\sqrt{4n^2\pi^2\Upsilon^2 - 1}$.

First, we restrict ourselves to the macroscopic regime where the Knudsen number is less than unity . As expected for $\eta = 100$ (steady state condition is satisfied), Fourier's law and the Cattaneo equation show the same linear temperature profiles (Figure (2.10)). A qualitative comparison of these equations for $\eta = 10$ has been shown in Figure (2.11). The influence of the temperature is sensed everywhere in the solid except near the regions $\varsigma = 1$. For $\eta = 1$ (see Figure (2.12)), the temperature profiles predicted by Fourier's law and the Cattaneo equation differ from each other. The Cattaneo equation shows a discontinuity in temperature profile. The wave front (located at ς_l) separates heated and unheated regions. For $\varsigma > \varsigma_l$ the temperature has not yet been sensed while behind the wave front ($\varsigma < \varsigma_l$), the Cattaneo temperature profile is higher than the Fourier temperature profile because the same amount of energy is exerted into a smaller volume of the film [21].

Temperature profiles for $Kn = 1$ and $\eta = 1$ have been illustrated in Figure (2.13). As previously mentioned, Fourier's law is not able to predict temperature profile in the mi-

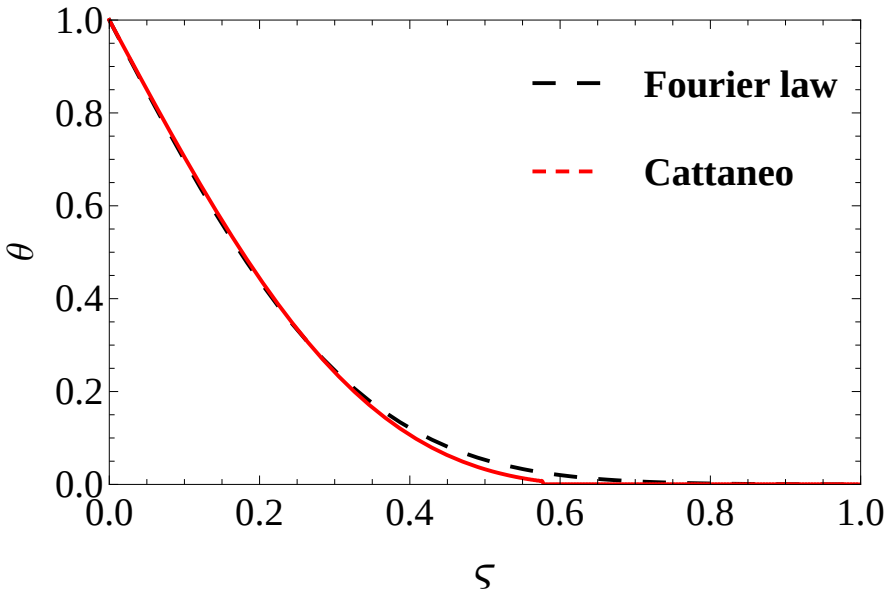

Figure 2.11: Temperature profile at $\eta = 10$ in macroscopic domain.

croscale domain. A linear temperature profile is predicted by Fourier's law even at smaller η. Again, the Cattaneo equation shows a jump in the temperature profile. Fourier's law and the Cattaneo equation are not able to predict temperature jump at the boundaries when $Kn \geq 1$. Effect of the purely ballistic regime on the temperature profile has been schematically described in Figure (2.14). Linear temperature profiles without any temperature jumps at the boundaries are predicted by Fourier's law, while the Cattaneo equation shows a discontinuity in predicting the temperature profile. A temperature jump can be seen for the Cattaneo equation, but it does not take place exactly at the boundaries. Therefore

i. Fourier's law and the Cattaneo equation are suitable to predict the temperature profile for macroscopic regimes; especially at steady state conditions where the Cattaneo equation tends to Fourier's law.

ii. Fourier's law is valid when the characteristic length scale is higher than the mean free path (i.e., macroscopic heat transfer).

iii. Fourier's law and the Cattaneo equation cannot be used to explain temperature profiles in a micro-scale regime (temperature jump at boundaries is not predicted).

iv. A discontinuity in temperature profile is predicted by the Cattaneo equation.

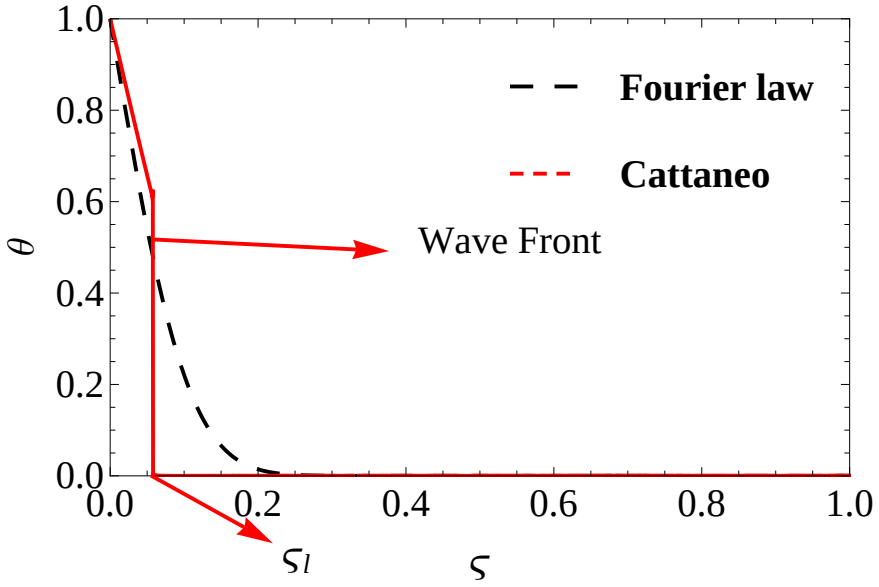

Figure 2.12: Temperature profile at $\eta = 1$ in macroscopic domain.

2.5.4 The equation of phonon radiative transfer (EPRT)

Using an analogy between phonon and photon, the Boltzmann transport equation can be expressed in terms of the phonon intensity defined as

$$\sin\theta\cos\phi\frac{\partial I}{\partial r} + \cos\theta\frac{\partial I}{\partial z} = -\frac{I - I_0}{\Lambda} \tag{2.54}$$

where the phonon intensity (I) is

$$I = \frac{1}{4}\sum v_r f \hbar\omega D(\omega) \tag{2.55}$$

By ϕ and θ, we denote azimuthal and polar angles, respectively [11, 17]. For steady state heat conduction in $r-$direction, the phonon intensity does not depend on $z-$direction. Therefore

$$\frac{\partial I}{\partial r} = -\frac{I - I_0}{\Lambda} \tag{2.56}$$

where $\mu = \cos\theta$ is directional cosine. The two-flux method is a helpful solution for the above equation. According to this method, the equations for forward $(+)$ and backward $(-)$ intensities can be written as

$$\frac{\partial I^-}{\partial r} = \frac{I_0 - I^-}{\Lambda}, \text{-1<}\mu\text{<0} \tag{2.57}$$

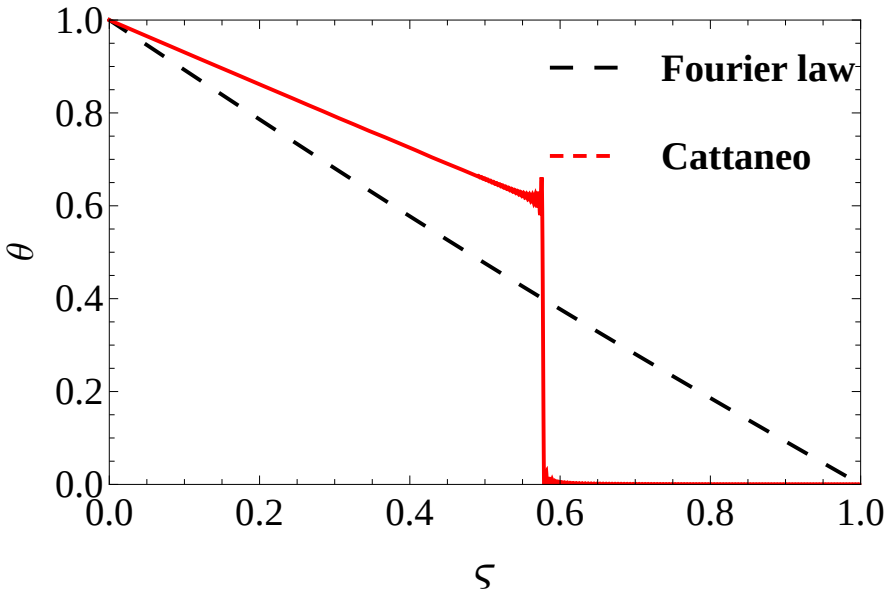

Figure 2.13: Temperature profile at $\eta = 1$ for $Kn = 1$.

$$\frac{\partial I^+}{\partial r} = \frac{I_0 - I^+}{\Lambda}, 0<\mu<1 \tag{2.58}$$

General solutions of equations (2.57) and (2.58) can be expressed as follows [11]

$$I^+(r,\mu) = I^+(0,\mu)\exp[\frac{-r}{\Lambda\mu}] - \int_0^r \exp[\frac{\xi - r}{\Lambda\mu}]I_0(\xi)\frac{d\xi}{\Lambda\mu} \tag{2.59}$$

$$I^-(r,\mu) = I^-(0,\mu)\exp[\frac{L - r}{\Lambda\mu}] - \int_r^L \exp[\frac{\xi - r}{\Lambda\mu}]I_0(\xi)\frac{d\xi}{\Lambda\mu} \tag{2.60}$$

The heat flux is written as

$$q = 2\pi \int_0^1 [I^+(r,\mu) - I^-(r,\mu)]\mu d\mu \tag{2.61}$$

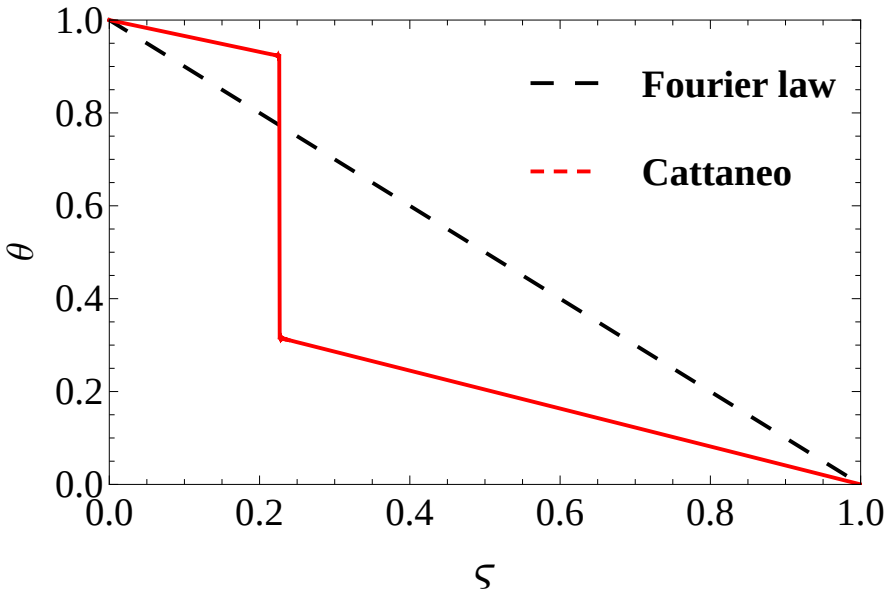

Figure 2.14: Temperature profile at $\eta = 1$ for $Kn = 10$.

Using equations (2.59) and (2.60) and the definition of the m^{th} exponential integral ($E_m(r) = \int_0^1 [\mu^{m-2} \exp[-r/\mu] d\mu]$), equation (2.61) yields

$$\frac{q}{2\pi} = I^+(0)E_3[\frac{r}{\Lambda}] - I^-(L)E_3[\frac{L-r}{\Lambda}] + \int_0^r E_2[\frac{r-\xi}{\Lambda}]I_0(\xi)\frac{d\xi}{\Lambda} - \int_r^L E_2[\frac{\xi-r}{\Lambda}]I_0(\xi)\frac{d\xi}{\Lambda} \quad (2.62)$$

In the acoustically thick limit, the first two terms in equation (2.62) can be dropped. Applying the first Taylor expansion $I_0(r) = I_0(\xi) + \frac{dI_0}{dr}(r-\xi) + ...$ and letting $z = (r-\xi)/\Lambda$ in the third and fourth terms, we have

$$\frac{q}{2\pi} = -\frac{dI_0}{dr}\Lambda(\int_0^\infty zE_2[z]dz + \int_0^{-\infty} zE_2[-z]dz) \quad (2.63)$$

Since $\int_0^\infty zE_2[z]dz = 1/3$, the heat flux becomes

$$q = -\frac{4\pi}{3}\Lambda\frac{dI_0}{dr} \quad (2.64)$$

For temperatures lower than the Debye temperature, the total intensity over the frequencies of interest is given by the Stefan-Boltzmann law.

$$I_0 = \frac{\sigma_{SB}}{\pi} T^4 \tag{2.65}$$

Where σ_{SB} is the Stefan-Boltzmann constant. Under the local thermal equilibrium condition, we can see [11, 16]

$$q = -\frac{16\sigma_{SB}T^3}{3}\Lambda\frac{dT}{dr} \tag{2.66}$$

This is a heat diffusion equation, if the thermal conductivity is defined as

$$k = \frac{16\sigma_{SB}T^3}{3}\Lambda \tag{2.67}$$

Comparing the thermal conductivity from the Boltzmann transport equation with the EPRT, we find that $Cv = 16\sigma_{SB}T^3$.

2.6 Thermal boundary resistance

Thermal resistance at the interface between two dissimilar materials is very important for heat transfer in heterostructures. The effect of the thermal boundary resistance manifests itself as a discontinuity in the temperature gradient because of a mismatch in phonon group velocity and the density of two dissimilar materials. The thermal boundary resistance can be greatly affected by the effective thermal conductivity [1, 4].
The thermal boundary conductance (inversely proportional to the thermal boundary resistance) is determined by the number of phonons occurring at the interface and the probability of each phonon being transmitted across the interface. The net heat flux transferring from one side (1) to the other (2) could be calculated by

$$q = h_B \Delta T \tag{2.68}$$

By h_B, we denote the thermal conductance at the boundary between two dissimilar materials [23]. There have been two famous theoretical models developed to predict thermal boundary resistance. The acoustic mismatch model (AMM) is used for the specular scattering of phonons at the interface and the diffuse mismatch model (DMM) was proposed to account for the diffuse scattering of phonons at the interface [24]. These models will be elucidated in this section [11, 25, 26].

The heat flux occurring at the interface can be expressed by

$$q_{interface} = \iint_{\Omega_1 > 2\pi} [t_{12} v_1 \cos\theta_1 \hbar\omega [f(\omega, T_{e1}) - f(\omega, T_{e2})] \frac{D_1(\omega)}{4\pi} d\omega] d\Omega_1 \tag{2.69}$$

where t_{12} is the phonon transmission probability from one side (1) to the other (2), $D_1(\omega)$ is the density of states, $f(\omega, T)$ is the Bose-Einstein phonon distribution function, ω is the phonon frequency, $d\Omega = 2\pi \sin\theta d\theta$ is the differential angle, and v is the phonon velocity [4, 11]. The rearranging equation (2.69) gives

$$q_{interface} = (T_{e1} - T_{e2}) \int_0^{2\pi} \int_0^{\pi/2} \int_0^{\omega_D} t_{12} v_1 \hbar\omega \frac{df}{dT} \frac{D_1(\omega)}{4\pi} \cos\theta_1 \sin\theta_1 d\omega d\theta_1 d\phi \tag{2.70}$$

where T_{e1} and T_{e2} are emitted temperatures for side (1) and (2), respectively. After some manipulation and using the definition of the volumetric specific heat capacity, the general equation for the thermal boundary resistance becomes [17]

$$\frac{1}{R} = \frac{1}{2} \int_0^1 t_{12}(\mu_1) C_1 v_1 \mu_1 d\mu_1 \tag{2.71}$$

where R is the thermal boundary resistance, and μ_1 is $\cos\theta_1$.

2.6.1 Diffuse mismatch model

The diffuse mismatch model theory was proposed by Swartz and Pohl [24] to predict the thermal boundary conductance. The diffuse mismatch model is established based on elastic scattering, that is, a phonon from side (1) with frequency ω only emits a phonon from the other side with same frequency. Also, according to the definition of diffuse scattering (the phonon loses its memory and forgets where comes from), the probability of reflection from one side is equal to the probability of transmission from the other side [26, 27]. It means that

$$t_{ji}^{(d)} = r_{ij}^{(d)} = 1 - t_{ij}^{(d)} \tag{2.72}$$

where $t_{ij}^{(d)}$ and $r_{ij}^{(d)}$ are the probabilities of transmission and reflection from side (i) to side (j), respectively. A balance of the total fluxes yields

$$t_{12}^{(d)} \int \hbar\omega v_1 D_1(\omega) f(\omega) d(\omega) = t_{21}^{(d)} \int \hbar\omega v_2 D_2(\omega) f(\omega) d(\omega) \tag{2.73}$$

Strictly speaking, within the limits of purely elastic scattering, a phonon from side (1) with frequency ω can only emit a phonon from the interface with the same frequency [26, 27]. Therefore, equation (2.73) can be written as:

$$t_{ij}^{(d)} = \frac{\sum_m v_{mj}^{-2}}{\sum_m v_{mi}^{-2} + \sum_m v_{mj}^{-2}} \tag{2.74}$$

where v_{mi} is the phonon group velocity of the m branch (m is transverse or longitudinal) in the i^{th} layer [24]. A similar relation can be obtained by using the relation between the phonon intensity and the volumetric specific heat capacity [16, 17]. The intensity of the phonon can be written as:

$$I_0 = \frac{Cv(T - T_{ref})}{4\pi} \tag{2.75}$$

where T_{ref} is a reference temperature. From equations (2.72), (2.73) and (2.75), the following expression for the probability of phonon transmission at the totally diffuse scattering limit is obtained [4].

$$t_{ij}^{(d)} = \frac{C_j v_j}{C_i v_i + C_j v_j} \tag{2.76}$$

This equation assumes that phonons of all frequencies in mediums (1) and (2) will participate in the thermal transmission. Therefore, a maximum transmission will occur in this condition [17]. Finally, for the totally diffuse interface, equation (2.71) is rearranged as

$$h_B^{(d)} = \frac{1}{R^{(d)}} = \frac{t_{12}^{(d)} C_1 v_1}{4} \tag{2.77}$$

where $h_B^{(d)}$ and $R^{(d)}$ are the diffuse thermal boundary conductance and the diffuse thermal boundary resistance, respectively.

2.6.2 Acoustic mismatch model

The interfacial thermal resistance is a function of phonon density of both mediums. In practice, when phonons are occurring at the interface, some of them are transmitted to the other side, while the rest of the phonons are reflected. This reflection can be specular (mirror like) or diffuse. The acoustic mismatch model is used to account for the specular scattering of phonons at the interface. The acoustic mismatch model is able to predict the interface properties at low temperatures, where the specular scattering is dominant [25, 28]. The degree of specularity of the phonons at the interface is determined

by

$$s = \exp[-\frac{16\pi^2\delta_{rms}^2}{\Delta^2}] \tag{2.78}$$

where s is the probability that phonons are scattered specularly at the surface, δ_{rms} and Δ are the asperity parameter of the interface and the coherence length, respectively. Δ is given by $\Delta = hv/k_BT$, where h is the Plank's constant, v is the phonon velocity and k_B and T are the Boltzmann's constant and temperature, respectively. The specular (smooth) interface is defined, if the specularity parameter is unity . By $s = 0$, the totally diffuse phonon scattering is satisfied. It is clear that temperature rising leads to increasing the probability of diffuse scattering [26, 27].

Calculation of the transmission probability and the thermal boundary resistance between two dissimilar materials is not a straightforward problem. In the acoustic mismatch model, the characteristic length scale of the interface roughness is assumed to be much smaller than the incident phonon wavelength. The acoustic mismatch model incorporates some simplifying assumptions. First, the phonons are governed by continuum acoustics, that is, the phonons are treated as plane waves in a continuous medium. Second, the interface is considered as a perfect plane [24].

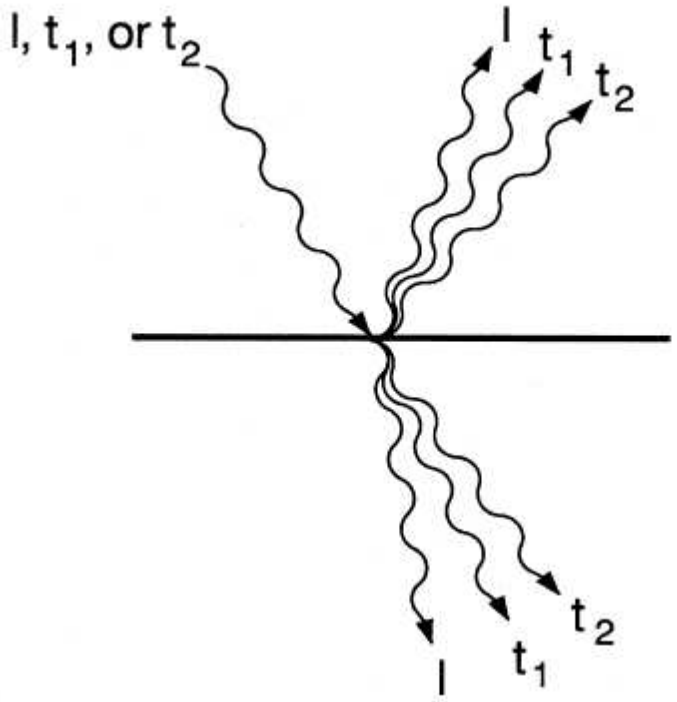

Figure 2.15: Schematic of many possibilities of a phonon incident at the interface between two dissimilar materials [24].

When a phonon is present at the interface, there are four general possible results as shown in Figure (2.15). The phonon can specularly reflect, reflect and mode convert, refract or refract and mode convert. The angles of reflection and refraction with or without mode converts are calculated by the acoustic analog of Snell's law for electromagnetic waves. Therefore, the angle of the transmitted phonon is determined by

$$\frac{\sin\theta_1}{v_1} = \frac{\sin\theta_2}{v_2} \tag{2.79}$$

We can consider two possibilities for equation (2.79). Considering the case $v_1 > v_2$, the Snell's law can be applied without restriction. In the opposite case, when $v_1 < v_2$, a critical angle θ_c, is defined. Above the critical angle ($\theta_1 > \theta_c$), total internal reflection occurs and the transmission probability vanishes completely ($t_{12}^{(s)} = 0$), while for the angle of incidence less than the critical angle, Snell's law is still valid. The simplest picture derivable from the acoustic mismatch model is presented by equation (2.80) in which the mode conversion at the interface is neglected and the velocities of all three polarizations are considered the same [29].

$$t_{12}^{(s)} = \frac{4\rho_1 v_1 \rho_2 v_2 \cos\theta_1 \cos\theta_2}{(4\rho_1 v_1 \cos\theta_1 + \rho_2 v_2 \cos\theta_2)^2} \tag{2.80}$$

Where $t_{12}^{(s)}$ is the probability of specular transmission, and ρ is the material density of each medium. In the totally specular limit, equation (2.71) can be written as

$$h_B^{(s)} = \frac{1}{R^{(s)}} = \frac{C_1 v_1}{2} \int t_{12}^{(s)}(\mu_1) d\mu_1 \tag{2.81}$$

where $h_B^{(s)}$ and $R^{(s)}$ are the specular thermal boundary conductance and the specular thermal boundary resistance, respectively.

The diffuse and specular thermal boundary resistance (equations (2.77 and 2.81)) were defined based on the temperature of the emitted phonons. It is worthwhile to note that the diffuse mismatch model discussed above is a simple approximation and not accurate when two mediums are very similar. Under this condition, the transmissivity should approach unity; but equation (2.74) predicts the probability of transmission approaching 0.5 and a finite value for the thermal boundary resistance is predicted in equation (2.77), even if the transmissivity sets $t_{12}^{(d)} = 1$. This dilemma arises from the temperature definition used in these equations. For heat conduction in micro and nano-scales where the Knudsen number is higher than 1, the local thermal equilibrium condition is no longer valid and

the temperature loses its conventional definition. So, the temperature is defined as the average energy of all phonons around the interface and is equivalent to the equilibrium temperature of those phonons, if they redistribute adiabatically to an equilibrium state. This temperature definition is not in coincidence with the definition of the emitted temperature. As illustrated in Figure (2.16), the equivalent equilibrium temperature on each side of the interface is not the same as that of the emitted temperature [4].

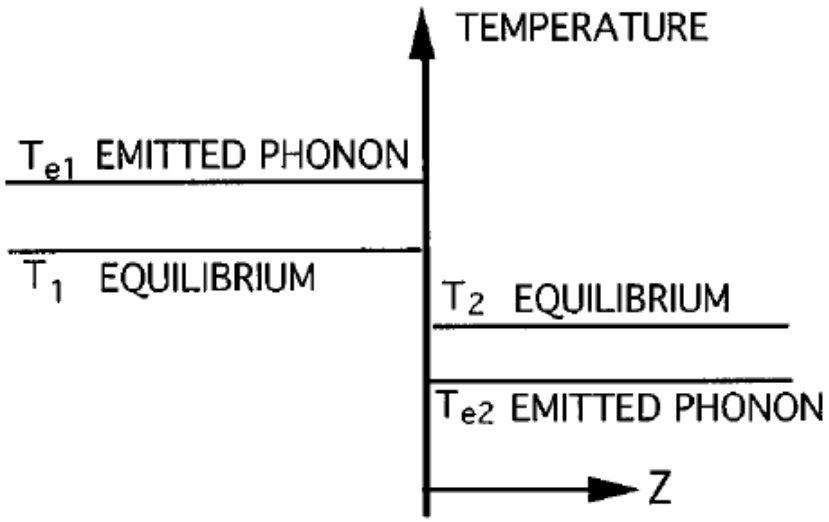

Figure 2.16: Equilibrium and emitted phonon temperature at interface between two dissimilar materials [4].

Therefore, the equivalent equilibrium temperature (T_1 and T_2) on each side of the interface can be shown in terms of T_{e1} and T_{e2} as

$$T_1 = T_{e1} - (T_{e1} - T_{e2}) \int t_{12}(\mu_1)\mu_1 d\mu_1 \tag{2.82}$$

and

$$T_2 = T_{e2} + (T_{e1} - T_{e2}) \int t_{21}(\mu_2)\mu_2 d\mu_2 \tag{2.83}$$

therefore

$$T_1 - T_2 = (T_{e1} - T_{e2})[1 - \int t_{12}(\mu_1)\mu_1 d\mu_1 - \int t_{21}(\mu_2)\mu_2 d\mu_2] \tag{2.84}$$

Based on the equivalent equilibrium temperature, the diffuse and specular thermal bound-

ary resistances are expressed as

$$R_d = \frac{4[1 - 0.5(t_{12}^{(d)} + t_{21}^{(d)})]}{t_{12}^{(d)} C_1 v_1} \tag{2.85}$$

and

$$R_s = \frac{2[1 - \int_0^1 t_{12}^{(s)}(\mu_1)\mu_1 d\mu_1 - \int_0^1 t_{21}^{(s)}(\mu_2)\mu_2 d\mu_2]}{C_1 v_1 \int_0^1 t_{12}^{(s)}(\mu_1)\mu_1 d\mu_1} \tag{2.86}$$

Thus, the diffuse and specular thermal boundary resistances based on the emitted and equivalent equilibrium temperatures are presented in Table 2.2 [4].

Table 2.2: thermal boundary resistance based on acoustic and diffuse mismatch models.

Thermal boundary resistance	Emitted temperature	Equivalent equilibrium temperature
Diffuse mismatch model	$\frac{4}{t_{12}^{(d)} C_1 v_1}$	$\frac{4[1-0.5(t_{12}^{(d)}+t_{21}^{(d)})]}{t_{12}^{(d)} C_1 v_1}$
Diffuse mismatch model	$\frac{2}{C_1 v_1 \int t_{12}^{(s)}(\mu_1) d\mu_1}$	$\frac{2[1-\int_0^1 t_{12}^{(s)}(\mu_1)\mu_1 d\mu_1 - \int_0^1 t_{21}^{(s)}(\mu_2)\mu_2 d\mu_2]}{C_1 v_1 \int_0^1 t_{12}^{(s)}(\mu_1)\mu_1 d\mu_1}$

2.7 Thermal conductivity of an inhomogeneous media using the generalized self consistent method

Consider a heterogeneous media comprising spherical particles suspended in a matrix. Generally, the effective thermal conductivity of a heterogeneous media is a function of particle size and shape, volume fraction, orientation and the thermal conductance at the interface between the matrix and suspended particles [30]. According to the phonon heat transfer approach, it is assumed that the thermal conductivity of the matrix and particles can be described based on the kinetic theory, i.e., $k = \frac{1}{3} C v \Lambda$. First, it is considered that the thermal conductivities of the matrix and suspended particles are the same as the corresponding bulk values. It means that the bulk mean free paths of the phonons are much smaller than the characteristic dimensions of the matrix and suspended particles. It is also assumed that the system is isotropic.

The volume average of the heat flux $< q >$ can be described by

$$< q >= -k_{eff}\frac{\Delta T}{L} \tag{2.87}$$

by ΔT, we denote the temperature difference between two faces of the system and L is the length of the sample. The volume average of the heat flux also can be obtained by another approach.

$$< q >= \phi_m < q >_m +\phi_p < q >_p \tag{2.88}$$

Where ϕ_m and ϕ_p are the volume fractions of the matrix and suspended particles, respectively. Here, $< q >_m$ and $< q >_p$ are the volume average of heat fluxes over the matrix and suspended particles, respectively. Substituting Fourier's law into the equation (2.88), we have

$$< q >= -\phi_m k_m < \nabla T >_m -\phi_p k_p < \nabla T >_p \tag{2.89}$$

Under the assumption of no discontinuities in the temperature field, it can be shown that

$$\frac{\Delta T}{L} = \phi_m < \nabla T >_m +\phi_p < \nabla T >_p \tag{2.90}$$

From equations (2.89) and (2.90), we have

$$< q >= -k_m\frac{\Delta T}{L} - \phi_p(k_p - k_m) < \nabla T >_p \tag{2.91}$$

Using equation (2.87), finally we obtain,

$$k_{eff}\frac{\Delta T}{L} = k_m\frac{\Delta T}{L} + \phi_p(k_p - k_m) < \nabla T >_p \tag{2.92}$$

The unknown parameter remaining in equation (2.92) is $< \nabla T >_p$. It is assumed that the spherical particle of radius r_p is embedded in a spherical matrix shell of radius r_m, which is surrounded by an infinite homogeneous media with effective thermal conductivity, k_{eff}. Also, there is no interaction between suspended particles. It means that each representative media comprises only one particle.

It is convenient to consider the steady state heat transfer to determine the temperature gradient inside the spherical particle. Laplace's equation is applied to calculate the temperature field.

$$\nabla^2 T_p = 0, 0 \leq r \leq r_p \tag{2.93}$$

$$\nabla^2 T_m = 0, r_p \leq r \leq r_m \tag{2.94}$$

$$\nabla^2 T_{eff} = 0, r_m \leq r \leq \infty \tag{2.95}$$

Where

$$\nabla^2 = \frac{1}{r^2}\frac{\partial}{\partial r}(r^2\frac{\partial}{\partial r}) + \frac{1}{r^2\sin\theta}\frac{\partial}{\partial\theta}(\sin\theta\frac{\partial}{\partial\theta}) \tag{2.96}$$

The following boundary conditions should be satisfied to conserve the continuity of the heat flux.

$$T_p(r,\theta) = finite \tag{2.97}$$

$$k_p\frac{\partial T_p(r_p,\theta)}{\partial r} = k_m\frac{\partial T_m(r_p,\theta)}{\partial r} \tag{2.98}$$

$$T_p(r_p,\theta) = T_m(r_p,\theta) \tag{2.99}$$

$$k_m\frac{\partial T_m(r_m,\theta)}{\partial r} = k_{eff}\frac{\partial T_{eff}(r_m,\theta)}{\partial r} \tag{2.100}$$

$$T_m(r_m,\theta) = T_{eff}(r_m,\theta) \tag{2.101}$$

$$T_{eff}(\infty,\theta) = -\alpha r\cos\theta \tag{2.102}$$

The temperature solutions can be written in the following simple form

$$T_p = A_2 r\cos\theta \tag{2.103}$$

$$T_m = (A_1 r + \frac{B_1}{r^2})\cos\theta \tag{2.104}$$

$$T_{eff} = (-\alpha r + \frac{B_0}{r^2})\cos\theta \tag{2.105}$$

Note that A_1, A_2, B_1 and B_0 are constants and should be determined. Substitution of the equations (2.103-2.105) into equations (2.97-2.102) is used to calculate the four unknown parameters. Finally, the particle temperature gradient is determined and represented by

$$< \nabla T >_p = A_2 = \frac{9k_m k_{eff}\frac{\Delta T}{L}}{[k_p + 2k_m](k_m + 2k_{eff}) + 2\phi_p[k_p - k_m](k_m - k_{eff})} \tag{2.106}$$

By inserting equation (2.106) into equation (2.92), finally the effective thermal conductivity of a heterogeneous media is determined.

$$k_{eff} = k_m\frac{2k_m + k_p + 2\phi_p(k_p - k_m)}{2k_m + k_p - \phi_p(k_p - k_m)} \tag{2.107}$$

In derivation of this equation, it is assumed that the interface between the matrix and suspended particles is perfect, i.e., no thermal boundary resistance at the interface. The

first two theoretical models to account for the thermal boundary resistance were proposed by Hasselman and Johnson [30] and Benveniste [31] with a different approach. Most recently, a new hetero-structure model for the effective thermal conductivity of composites comprising the thermal boundary resistance was presented by Nan et al. [32]. This model has the following form,

$$k_{eff} = k_m \frac{2k_m + k_p(1+2\alpha) + 2\phi_p(k_p(1-\alpha) - k_m)}{2k_m + k_p(1+2\alpha) - \phi_p(k_p(1-\alpha) - k_m)} \tag{2.108}$$

where α is a dimensionless parameter to introduce the thermal boundary resistance effects, i.e., $\alpha = \frac{a_K}{a_p}$, where a_p is the radius of the spherical particle and a_K is the thickness of the matrix-filled layer surrounding the particle in which the same temperature drop occurs as that at the interface, defined as

$$a_k = Rk_m \tag{2.109}$$

Note that R is the thermal boundary resistance. If $a_K = 0$ and thus $\alpha = 0$ then the interface is called a perfect interface. Although these models had some privileges as compared to that model with the perfect boundary resistance, they were still unable to predict the effective thermal conductivity of nanocomposites.

Chapter 3

Details about the modeling process

3.1 Effective Thermal conductivity of the matrix

Based on the phonon transport theory, the thermal conductivity of materials can be estimated from the bulk mean free path Λ, the volumetric specific heat C, and the phonon group velocity v:

$$k = \frac{1}{3}\int C(\omega)v(\omega)\Lambda(\omega)d\omega \approx \frac{1}{3}Cv\Lambda \tag{3.1}$$

For a heterogeneous media (spherical particles suspended in a matrix), the mean free path of the phonons is affected by interfacial scattering. The effective mean free path is defined for both matrix and particle phases. Under the assumption that the scattering mechanisms are independent of each other, Matthiessen's rule is applied. According to Matthiessen's rule, the effective mean free path, $\Lambda_{eff,m}$ of the matrix is defined as follows:

$$\frac{1}{\Lambda_{eff,m}} = \frac{1}{\Lambda_{b,m}} + \frac{1}{\Lambda_{coll}} + \frac{1}{\Lambda_{TBR}} + ... \tag{3.2}$$

where $\Lambda_{b,m}$ and Λ_{coll} are the bulk mean free path of the matrix and the mean free path of the phonon-particle collision, respectively. Λ_{TBR} is defined as the thermal boundary resistance mean free path due to matrix-particle interfaces. As expected, the mean free path of phonons in the matrix decreases due to the existence of the particles. Spherical particles of radius a_p are considered to be embedded in a representative medium of the matrix with effective cell length a (a is the average length of a side of a cube comprising only one particle). The volume fraction ϕ_p of particles in the matrix phase is

$$\phi_p = \frac{\frac{4}{3}\pi a_p^3}{a^3} \tag{3.3}$$

The collision mean free path is the distance traveled by phonons divided by the number of collisions. Now, if a phonon travels distance L (see Figure (3.1)), it will have $N = (n\pi a_p^2 L)$ collisions with particles [33, 34], where n is the density of particles defined as the number of particles per unit volume of the composite, i.e., $n = 1/a^3$. Finally, the collision mean free path is defined as

$$\Lambda_{coll} = \frac{L}{n\pi a_p^2 L} = \frac{a^3}{\pi_p a_p^2} = \frac{4a_p}{3\phi_p} \tag{3.4}$$

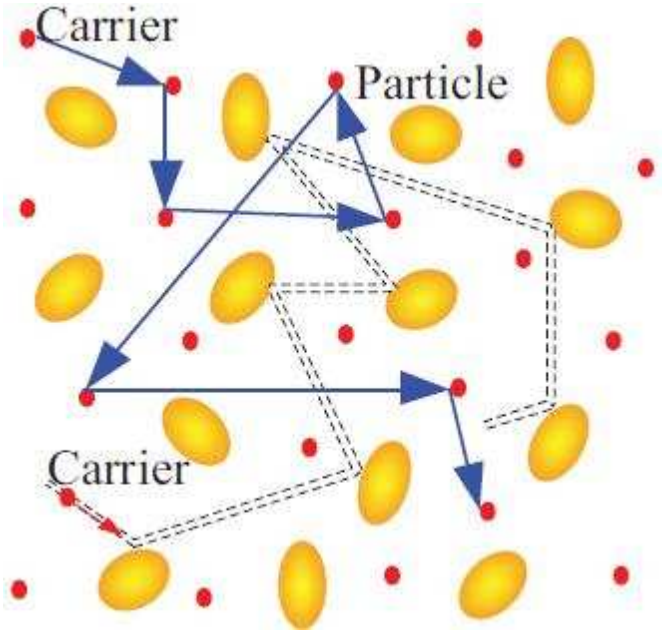

Figure 3.1: Schematic showing phonon-particle collision in an inhomogeneous media [34].

Considering the probability of specular reflection (s) of phonons from the particle surface, the specularity parameter is applied to alter the radius to an effective radius [35, 36]. Thus, the effective particle radius is

$$a_p^{(s)} = a_p \frac{1+s}{1-s} \tag{3.5}$$

And, consequently, the general equation for the collision mean free path is derived.

$$\Lambda_{coll} = \frac{4a_p^{(s)}}{3\phi_p} \tag{3.6}$$

Where the probability that the phonon is scattered specularly at the interface is determined by the value of s. In practice, the interface surface roughness is an important parameter to determine the value of the specularity parameter. Purely diffuse phonon scattering is satisfied, when $s = 0$. It is remarkable to note that the pure specular collision (i.e. for the case $s = 1$) is equivalent to $a_p^{(s)} \to \infty$ or no resistance due to the particle size effect [35].

The thermal boundary resistance in diffuse and specular limits was presented in Table (2.2). Using these expressions and definition of thermal conductivity based on the kinetic theory (see equation (3.1)), we reach the following expressions for the transmission mean free path in the diffuse and specular phonon scatterings (see Table 3.1).

Table 3.1: Derived transmission lengths for different boundary resistances.

Transmission mean free path	Emitted temperature	Equivalent equilibrium temperature
Diffuse ($\Lambda^{(d)}$)	$\frac{3a_K^{(d)}t_{mp}^{(d)}}{4}$	$\frac{3a_K^{(d)}t_{d,mp}}{4[1-0.5(t_{mp}^{(d)}+t_{pm}^{(d)})]}$
Specular ($\Lambda^{(s)}$)	$\frac{3a_K^{(s)}\int_0^1 t_{mp}^{(s)}(\mu_m)\mu_m d\mu_m}{2}$	$\frac{3a_K^{(s)}\int_0^1 t_{mp}^{(s)}(\mu_m)\mu_m d\mu_m}{2[1-\int_0^1 t_{mp}^{(s)}(\mu_m)\mu_m d\mu_m-\int_0^1 t_{pm}^{(s)}(\mu_p)\mu_p d\mu_p]}$

Where $a_K^{(d)} = k_m R^{(d)}$ and $a_K^{(s)} = k_m R^{(s)}$ are known as diffuse and specular Kapitza lengths, respectively. $\Lambda^{(d)}$ and $\Lambda^{(s)}$ are the totally diffuse and the totally specular transmission mean free paths, respectively. The Kapitza length is the thickness of the matrix phase, which is thermally equivalent to the interface. In other words, the Kapitza length is defined as the thickness of the bulk medium in which the same temperature drop occurs as that at the interface [37].

Depending on the ratio of the particle radius to the bulk Kapitza length, the thermal conductivity of the composite can increase or decrease with the volume fraction of the particles. For $\frac{a_p}{a_K} \geq 1$, the thermal conductivity increases with ϕ_p, while for $\frac{a_p}{a_K} \leq 1$, it decreases with ϕ_p [38].

The effective area for a collision between a phonon and a spherical particle is (πa_p^2), so if a phonon travels the Kapitza length for transmission, it will have $n(\pi a_p^2 a_K)$ transmissions. Where n is the density of particles (the number of particles per unit volume of the composite), thus the volume fraction is $\phi_p = 4n\pi a_p^3/3$.

The thermal boundary resistance mean free path is defined as the ratio of the transmission mean free path to the number of transmissions, with the assumption that a phonon travels the Kapitza length to transmit from the matrix to the particle. Therefore, the thermal boundary resistance mean free path under the totally diffuse ($\Lambda_{TBR}^{(d)}$) and the totally specular ($\Lambda_{TBR}^{(s)}$) limits can be written by

$$\Lambda_{TBR} = \begin{cases} \frac{a_p t_{mp}^{(d)}}{\phi_p[1-0.5(t_{mp}^{(d)}+t_{pm}^{(d)})]}, & \text{totally diffuse} \\ \\ \frac{2a_p\int_0^1 t_{mp}^{(s)}(\mu_m)\mu_m d\mu_m}{\phi_p[1-\int_0^1 t_{mp}^{(s)}(\mu_m)\mu_m d\mu_m-\int_0^1 t_{pm}^{(s)}(\mu_p)\mu_p d\mu_p]}, & \text{totally specular} \end{cases} \tag{3.7}$$

Furthermore, the specular and diffuse thermal boundary resistance mean free paths based

on the emitted temperature are presented.

$$\Lambda_{TBR} = \begin{cases} \frac{a_p t_{mp}^{(d)}}{\phi_p}, \text{ totally diffuse} \\ \\ \frac{2a_p \int_0^1 t_{mp}^{(s)}(\mu_m)\mu_m d\mu_m}{\phi_p}, \text{ totally specular} \end{cases} \tag{3.8}$$

Applying the collision and the thermal boundary resistance mean free paths for the specular and diffuse phonon scattering for the emitted and equivalent equilibrium temperatures, the effective mean free path of the matrix phase can be calculated by Matthiessen's rule (equation(3.2)). Alternatively, we can write Matthiessen's rule in the form of

$$\Lambda_{eff,m} = F_m^{(\Xi)} \Lambda_{b,m}, \Xi{=}d, s \tag{3.9}$$

where F_m is the scaling factor coefficient and the upper index "Ξ" stands for the diffuse (d) and specular (s) phonon scattering.
Therefore, the specular and diffuse scaling factor coefficients for the matrix phase for the emitted and equivalent equilibrium temperatures are determined. For the diffuse scaling factor, we have

$$F_m^{(d)} = \begin{cases} \frac{4\frac{a_p}{\Lambda_{b,m}} t_{mp}^{(d)}}{4\frac{a_p}{\Lambda_{b,m}} t_{mp}^{(d)} + \phi_p[3t_{mp}^{(d)}+4]}, \text{ emitted temperature} \\ \\ \frac{4\frac{a_p}{\Lambda_{b,m}} t_{mp}^{(d)}}{4\frac{a_p}{\Lambda_{b,m}} t_{mp}^{(d)} + \phi_p[t_{mp}^{(d)}-2t_{pm}^{(d)}+4]}, \text{ equivalent equilibrium temperature} \end{cases} \tag{3.10}$$

Similarly, the scaling factor for the specular phonon scattering is presented as

$$F_m^{(s)} = \begin{cases} \frac{4\frac{a_p}{\Lambda_{b,m}} \int_0^1 t_{mp}^{(s)}(\mu_m)\mu_m d\mu_m}{4\frac{a_p}{\Lambda_{b,m}} \int_0^1 t_{mp}^{(s)}(\mu_m)\mu_m d\mu_m + \phi_p[3\frac{a_p}{a_p^{(s)}} \int_0^1 t_{mp}^{(s)}(\mu_m)\mu_m d\mu_m + 2]}, \text{ emitted temperature} \\ \\ \frac{4\frac{a_p}{\Lambda_{b,m}} \int_0^1 t_{mp}^{(s)}(\mu_m)\mu_m d\mu_m}{4\frac{a_p}{\Lambda_{b,m}} \int_0^1 t_{mp}^{(s)}(\mu_m)\mu_m d\mu_m + \phi_p[2(1-\int_0^1 t_{pm}^{(s)}(\mu_m)\mu_m d\mu_m) + \int_0^1 t_{mp}^{(s)}(\mu_p)\mu_p d\mu_p(\frac{3a_p}{a_p^{(s)}}-2)]}, \\ \text{equivalent equilibrium temperature} \end{cases} \tag{3.11}$$

Substituting equations (3.10) and (3.11) into equation (3.9), the effective mean free paths of the matrix phase under the specular and diffuse phonon-particle scatterings are deter-

mined and, consequently, the effective thermal conductivity of the matrix is obtained.

$$k_{eff,m}^{(\Xi)} = \frac{1}{3} C_m v_m \Lambda_{eff,m}^{(\Xi)}, \Xi = s, d \tag{3.12}$$

3.2 Effective thermal conductivity of the suspended particles

The thermal conductivity of micro- and nano-structures differs significantly from corresponding bulk materials. This reduction creates some significant problems in instruments where efficient heat removal is an important issue. However, it is beneficial when low thermal conductivity is required.

In small scale regimes, the boundary effect becomes important and it is caused a reduction in the effective thermal conductivity of the media. Different types of scattering mechanisms can participate in the effective mean free path. Again, Matthiessen's rule is used to describe the contribution of the scattering mechanisms in the heat transfer [6, 7].

The conventional concept of the thermal conductivity breaks down when the characteristic length of the media (i.e., diameter for spherical particles and wires, thickness for the thin film) is smaller than the bulk mean free path. On the other hand, the boundary scattering becomes significant for the Knudsen number greater than unity [39].

Thus, it would be considered that the effective mean free path of a nano-scale material is a function of the bulk mean free path and the characteristic length of the media [33]. Recalling Matthiessen's rule, an effective mean free path of the suspended nanoparticle is taken into account.

$$\frac{1}{\Lambda_{eff,p}} = \frac{1}{\Lambda_{b,p}} + \frac{1}{2a_p^{(s)}} \tag{3.13}$$

Where $\Lambda_{b,p}$ is the bulk mean free path of the suspended particles and $a_p^{(s)}$ is the effective radius of the particle. Note that for the diffuse phonon boundary scattering $a_p^{(s)} \equiv a_p$, while there is no boundary scattering resistance in the case of the completely specular scattering. Rewriting equation (3.13) in the spirit of equation (3.9), the scaling factor for the suspended particle is determined.

$$F_p = \frac{\frac{2a_p^{(s)}}{\Lambda_{b,p}}}{\frac{2a_p^{(s)}}{\Lambda_{b,p}} + 1} \tag{3.14}$$

It is clear that the particle scaling factor is unity (i.e., $F_p = 1$) for the pure specular boundary scattering. On the other hand, the boundary scattering resistance is neglected and only the internal resistance contributes to a reduction in the thermal conductivity. Chen [39] proposed an analytical formula to determine the effective thermal conductivity of the nano-spherical particles. This equation provides almost the same results as that by the exact solution of the Boltzmann transport equation. We rearrange this equation in the form of Matthiessen's rule as follows:

$$\frac{1}{\Lambda_{eff,p}} = \frac{1}{\Lambda_{b,p}} + \frac{4}{3a_p^{(s)}} \tag{3.15}$$

Thus, using the above equation, the scaling factor for the particle phase is defined.

$$F_p = \frac{\frac{3a_p^{(s)}}{4\Lambda_{b,p}}}{\frac{3a_p^{(s)}}{4\Lambda_{b,p}} + 1} \tag{3.16}$$

Finally, the effective thermal conductivity of the suspended particle is expressed as

$$k_{eff,p}^{(\Xi)} = \frac{1}{3} C_p v_p \Lambda_{eff,p}^{(\Xi)}, \Xi = s, d \tag{3.17}$$

3.3 Effective thermal conductivity of the thin films

The thermal conductivity of a thin film is investigated in this section (see Figure(3.2)). The steady state Boltzmann transport equation is written [11, 20].

$$v_x \frac{\partial f}{\partial x} + v_z \frac{\partial f}{\partial z} = \frac{f_0 - f}{\tau} \tag{3.18}$$

The phonon distribution function, f, is

$$f = f_0 + \epsilon \tag{3.19}$$

where ϵ is the deviation from the equilibrium distribution (f_0). It is assumed that the local thermal equilibrium (temperature gradient) is established in the x-direction. Thus,

$$v_x \frac{dT}{dx} \frac{df_0}{dT} + v_z \frac{\partial \epsilon}{\partial z} = \frac{-\epsilon}{\tau} \tag{3.20}$$

In derivation equation (3.20), it is assumed that there is no temperature gradient in the y- and z-directions, thus $\frac{\partial f_0}{\partial z} = \frac{\partial f_0}{\partial y} = 0$. It is also assumed that the film is infinite in the y-direction. However, $\frac{\partial \epsilon}{\partial y} = 0$. Finally $\frac{\partial \epsilon}{\partial x}$ is neglected as compared to $\frac{\partial f_0}{\partial x}$. Considering $(v_x \frac{\partial T}{\partial x} \frac{\partial f_0}{\partial T})^{-1} = \tau_0$, the solution to equation (3.20) is

$$\epsilon(z) = A \exp(\frac{-z}{v_z \tau}) - \frac{\tau}{\tau_0} \tag{3.21}$$

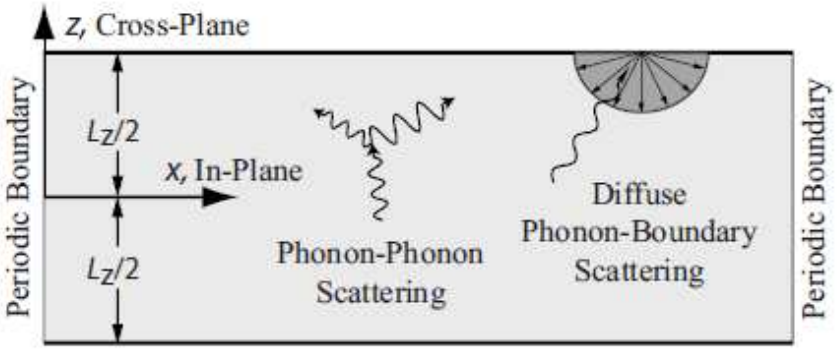

Figure 3.2: Schematic diagram of the thin film. The film is finite in the z-direction and periodic in the x- and y-directions [6].

The distribution function of phonons leaving the surface ($z = -\frac{L}{2}$) is given by

$$f^+(v_z^+, -\frac{L}{2}) = s f^-(v_z^-, -\frac{L}{2}) + (1-s) f_0 \tag{3.22}$$

and similarly, at $z = \frac{L}{2}$

$$f^-(v_z^-, \frac{L}{2}) = s f^+(v_z^+, \frac{L}{2}) + (1-s) f_0 \tag{3.23}$$

It means that phonons traveling toward boundaries are either specularly reflected with probability s or scattered into the equilibrium distribution with probability $1 - s$ [40]. Substituting equation (3.19) into equations (3.22) and (3.23), finally we have

$$\epsilon^+(v_z^+, -\frac{L}{2}) = s\epsilon^-(v_z^-, -\frac{L}{2}) \tag{3.24}$$

and

$$\epsilon^-(v_z^-, \frac{L}{2}) = s\epsilon^+(v_z^+, \frac{L}{2}) \tag{3.25}$$

The upper index (+) denotes a phonon traveling toward the surface located at $z = L/2$ and the upper index (−) denotes a phonon traveling toward the surface located at $z = -L/2$. Note that the boundary scattering is elastic (i.e. $v_z^+ = -v_z^-$). Applying boundary conditions (equations (3.24) and (3.25)) into equation (3.21) and the elimination of $\epsilon^-(-\frac{L}{2})$ and $\epsilon^+(\frac{L}{2})$ yields

$$\epsilon^{\pm}(z) = \frac{\tau}{\tau_0}\exp(\frac{-L \mp 2z}{2v_z\tau})\frac{1-s}{1-s\exp(-\frac{L}{v_z\tau})} - \frac{\tau}{\tau_0} \tag{3.26}$$

The heat flux in x-direction can be defined as

$$q_x = \hbar\omega v_x \bar{\epsilon} \tag{3.27}$$

where $\bar{\epsilon} = \frac{\int_{-L/2}^{L/2}\epsilon(z)dz}{\int_{-L/2}^{L/2}dz}$. Therefore,

$$q_x = -\hbar\omega v_x \frac{\tau}{\tau_0}F \tag{3.28}$$

where F is the scaling factor given by

$$F = 1 - \frac{1-s}{L/\Lambda_b}\frac{1-\exp(-L/\Lambda_b)}{1-s\exp(-L/\Lambda_b)} \tag{3.29}$$

Note the bulk mean free path $\Lambda_b = \tau v_z$. Consequently, the in-plane thermal conductivity of the thin film is

$$k = \frac{q_x}{\partial T/\partial x} = \frac{1}{3}Cv\Lambda_b F \tag{3.30}$$

In the above derivation, the thin film is assumed as an isotropic material, i.e., the atomic crystal is uniform in all directions. Therefore, the phonon group velocities in all directions are the same [41]. Also, different approaches have been introduced to obtain the effective thermal conductivity of the thin film [19, 42]. Note that phonon transport is confined by scattering with the boundaries of the thin film and, subsequently, the effective thermal conductivity becomes size dependent [43].

Under the assumption that the scattering mechanisms are independent of each other, Matthiessen's rule is applied [44]. Matthiessen's rule can also be used to determine the effective mean free path and, consequently, the effective thermal conductivity of the thin film in the x-direction.

$$\frac{1}{\Lambda_{eff,thinfilm}} = \frac{1}{\Lambda_b} + \frac{1-s}{L(1+s)} \tag{3.31}$$

Rewriting equation (3.31) in the spirit of equation (3.9), the obtained scaling factor from Matthiessen's rule F_M is

$$F_M = \frac{\frac{L(1+s)}{\Lambda_b}}{\frac{L(1+s)}{\Lambda_b} + (1-s)} \tag{3.32}$$

and

$$k = \frac{1}{3} C v \Lambda_b F_M \tag{3.33}$$

where L is the film thickness. In Figure (3.3), thickness dependence of the thermal con-

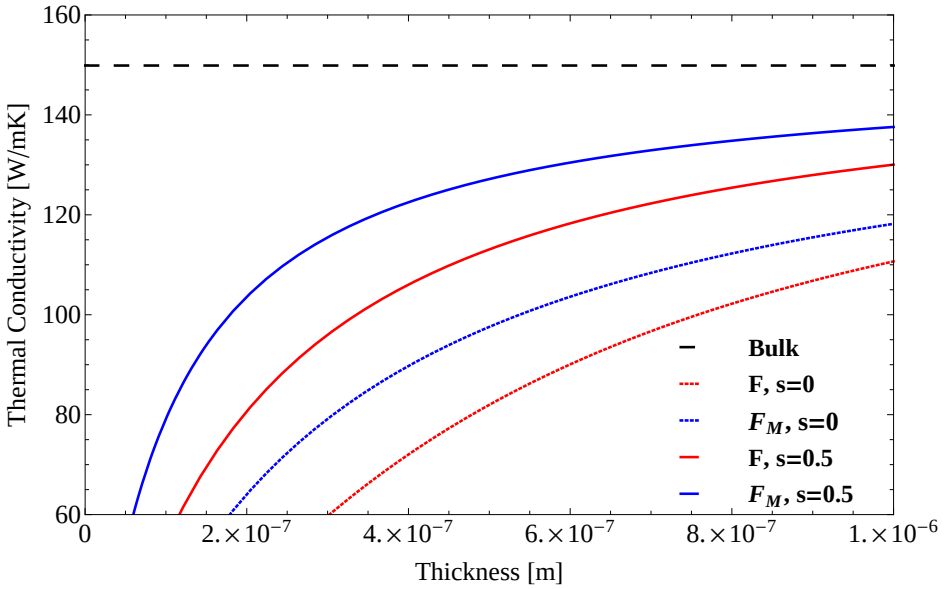

Figure 3.3: Thickness dependence of the thermal conductivity of the silicon films.

ductivities of the silicon films resulting from equations (3.30) and (3.33) are compared to the bulk thermal conductivity. The effect of the boundary scattering is neglected when the film thickness is greater than the bulk phonon mean free path (i.e., $Kn < 1$). It means that the thermal conductivity of the thin film tends to the corresponding bulk thermal conductivity. The effective thermal conductivities resulting from equation (3.30) predict smaller values than those resulting from equation (3.33), since independent scattering mechanisms are considered in Matthiessen's rule. In the case of the perfect specular boundary scattering (i.e., $s = 1$), the effective thermal conductivity of the thin film is the same as the corresponding bulk value. In contrast, the diffuse boundary scattering (i.e., $s = 0$) predicts the smallest thermal conductivity due to phonon transport confinement. By doing some modifications to the scaling factor coefficient (equation (3.29)), the effective thermal conductivity of the thin film in the longitudinal direction will be modified.

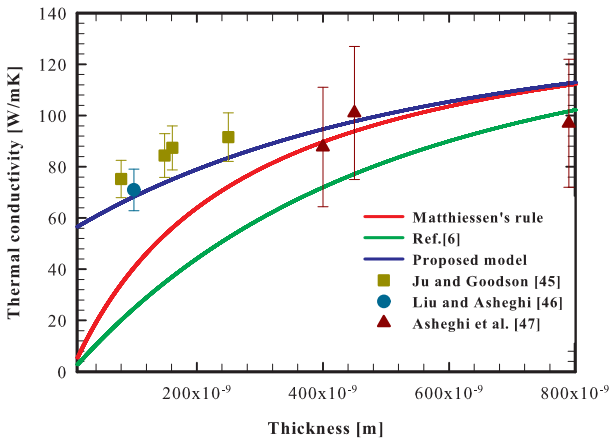

Figure 3.4: In-plane thermal conductivity of the silicon thin film as a function of the thickness. Our results are in good agreement with experimental results.

Considering the boundary scattering effect, the phonon bulk mean free path (Λ_b) is replaced by the effective mean free path, (Λ_{eff}). Mathiessen's rule is used to determine the effective mean free path (see equation (3.31)). Finally we reach the following equation for the scaling factor

$$F = 1 - \frac{1-s}{L/\Lambda_{eff}} \frac{1-\exp(-L/\Lambda_{eff})}{1-s\exp(-L/\Lambda_{eff})} \tag{3.34}$$

And, consequently, the in-plane thermal conductivity of the thin film is presented as follows:

$$k = \frac{1}{3} C v \Lambda_b \left(1 - \frac{1-s}{L/\Lambda_{eff}} \frac{1-\exp(-L/\Lambda_{eff})}{1-s\exp(-L/\Lambda_{eff})}\right) \tag{3.35}$$

In Figure (3.4), the longitudinal thermal conductivity of a thin film of silicon as a function of the thickness has been illustrated. Our results (see (3.35)) are compared with the experimental data [45–47], analytical results [6] and Matthiessen's rule for the diffuse boundary scattering (i.e., $s = 0$). The proposed model for the effective thermal conductivity of the silicon thin film agrees well with experimental results, especially for a lesser thickness.

3.4 Generic formula for the thermal conductivity in particulate nanocomposites

In fact, any phonon scattering mechanism in a more general case can be treated as partially specular-partially diffuse, which can be quantified by the probability of specular reflection

(s).

$$k_{eff} = sk_{eff}^{(s)} + (1-s)k_{eff}^{(d)} \tag{3.36}$$

where

$$\begin{aligned}
&k_{eff}^{(i)} \\
&= \frac{1}{3}C_m v_m \Lambda_{b,m} F_m^{(i)} \\
&\times \frac{\frac{2}{3}C_m v_m \Lambda_{b,m} F_m^{(i)} + \frac{1}{3}C_p v_p \Lambda_{b,p} F_p^{(i,1)} + 2\phi_p \left(\frac{1}{3}C_p v_p \Lambda_{b,p} F_p^{(i,2)} - \frac{1}{3}C_m v_m \Lambda_{b,m} F_m^{(i)}\right)}{\frac{2}{3}C_m v_m \Lambda_{b,m} F_m^{(i)} + \frac{1}{3}C_p v_p \Lambda_{b,p} F_p^{(i,1)} - \phi_p \left(\frac{1}{3}C_p v_p \Lambda_{b,p} F_p^{(i,2)} - \frac{1}{3}C_m v_m \Lambda_{b,m} F_m^{(i)}\right)} \\
&i = s, d
\end{aligned} \tag{3.37}$$

3.4.1 Minnich-Chen formula

Now, we can present specific cases of the generic formula. In the Minnich and Chen formula, scaling factors are presented as,

$$\begin{aligned}
F_m^{(d)} &= \frac{2\frac{2a_p}{\Lambda_{b,m}}}{2\frac{2a_p}{\Lambda_{b,m}} + 3\phi_p} \\
F_p^{(d,1)} &= \left(\frac{\frac{2a_p}{\Lambda_{b,p}}}{\frac{2a_p}{\Lambda_{b,p}} + 1}\right)(1 + 2\alpha(\phi_p, a_p)) \\
F_p^{(d,2)} &= \left(\frac{\frac{2a_p}{\Lambda_{b,p}}}{\frac{2a_p}{\Lambda_{b,p}} + 1}\right)(1 - \alpha(\phi_p, a_p))
\end{aligned} \tag{3.38}$$

Note that the Minnich-Chen formula does not consider the specular phonon scattering. Thus, $F_m^{(s)} = 0, F_p^{(s,1)} = 0, F_p^{(s,2)} = 0$, and purely diffuse scattering is only described. Traditional dimensionless thermal boundary resistance, α was presented based on the emitted temperature at the interface between the matrix and suspended particles. It means that the thermal boundary resistance is given by

$$R = 4\left(\frac{C_m v_m + C_p v_p}{C_m v_m C_p v_p}\right) \tag{3.39}$$

And, consequently, α is expressed in the following form

$$\alpha(\phi_p, a_p) = \frac{4\Lambda_m}{3a_p}\left(\frac{C_m v_m + C_p v_p}{C_p v_p}\right) F_m^{(d)} \tag{3.40}$$

3.4.2 Novel formula

Derivation of the Minnich-Chen formula does not include the specular scattering of phonons on the particle-matrix interface. The alternative derivation in this section allows taking into account more details of phonon collisions. Our starting point is equation (2.107) which is used for the perfect interface between matrix and particles. In our model, the effect of the thermal boundary resistance is presented in terms of the effective phonon mean free path. Also, we present our results based on the equivalent equilibrium temperature, which is more realistic than the emitted temperature assumption [4]. The specular and partially specular-partially diffuse phonon scatterings also are included in our formula.

Our novel formula is presented by equations (3.36) and (3.37) using the following scaling coefficients

$$F_p^{(i,1)} = F_p^{(i,2)};\ i = s, d$$

$$F_m^{(d)} = \frac{4\frac{a_p}{\Lambda_{b,m}} t_{mp}^{(d)}}{4\frac{a_p}{\Lambda_{b,m}} t_{mp}^{(d)} + \phi_p[t_{mp}^{(d)} - 2t_{pm}^{(d)} + 4]}$$

$$F_m^{(s)} = 4\frac{a_p}{\Lambda_{b,m}} \int_0^1 t_{mp}^{(s)}(\mu_m)\mu_m d\mu_m /$$

$$4\frac{a_p}{\Lambda_{b,m}} \int_0^1 t_{mp}^{(s)}(\mu_m)\mu_m d\mu_m + \phi_p[2(1 - \int_0^1 t_{pm}^{(s)}(\mu_m)\mu_m d\mu_m) + \int_0^1 t_{mp}^{(s)}(\mu_p)\mu_p d\mu_p(\frac{3a_p}{a_p^{(s)}} - 2)]$$

$$F_p^{(d)} = \frac{3\frac{a_p}{\Lambda_{b,p}}}{3\frac{a_p}{\Lambda_{b,p}} + 4}$$

$$F_p^{(s)} = 1 \tag{3.41}$$

Chapter 4

Discussion

Discussion

In Figure (4.1), the specular and diffuse scaling factor coefficients are plotted as a function of the volume fraction for different particle sizes. The specular and diffuse scaling factors decrease monotonically by increasing the volume fraction due to the relative increasing phonon-particle collision area per unit volume. Increasing particle size leads to a decrease in the effective area for phonon-particle scattering and, consequently, higher values for the scaling factors are predicted. Note that the specular scaling factor always predicts higher values than the diffuse one due to smaller phonon transport confinement.

Figure (4.2) shows the effective thermal conductivity of the matrix depends on whether

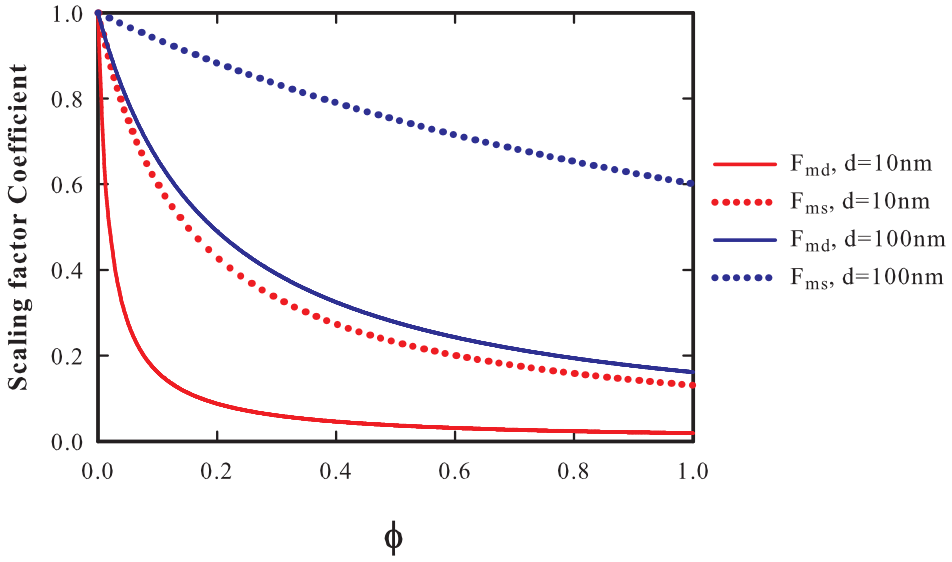

Figure 4.1: The totally specular and totally diffuse scaling factors plotted as a function of the volume fraction for various particle sizes.

phonons are scattered specularly or diffusely at the interface. Diffuse phonon scattering causes a drastic reduction in the effective thermal conductivity because of the diffuse interface scattering is always more effective than the specular scattering at confining the phonon transport.

Similar results are observed for the effective thermal conductivity of the suspended particles (see Figure (4.3)). For higher values of the specularity parameter (s), the effective thermal conductivity of the particle is more sensitive to changes in s. These changes are more significant for the smaller particle sizes due to the greater density of the interface [18, 48]. In the case of the specular boundary scattering (i.e., $s = 1$), the effective

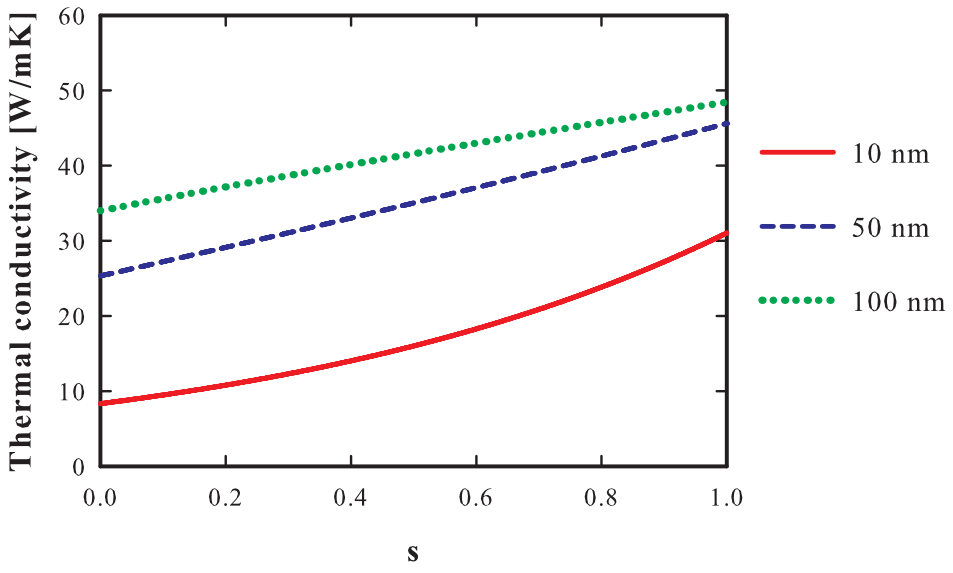

Figure 4.2: Interfacial specularity dependency of the thermal conductivity of the matrix phase in different particle sizes when $\phi = 0.1$.

radius, $a_p^{(s)}$ tends to infinity (i.e., no resistance due to particle size effect). However, the confinement of phonon transport is less than the diffuse boundary scattering. It is remarked that the effect of the boundary scattering is neglected as compared to the internal thermal resistance for the specular phonon transport.

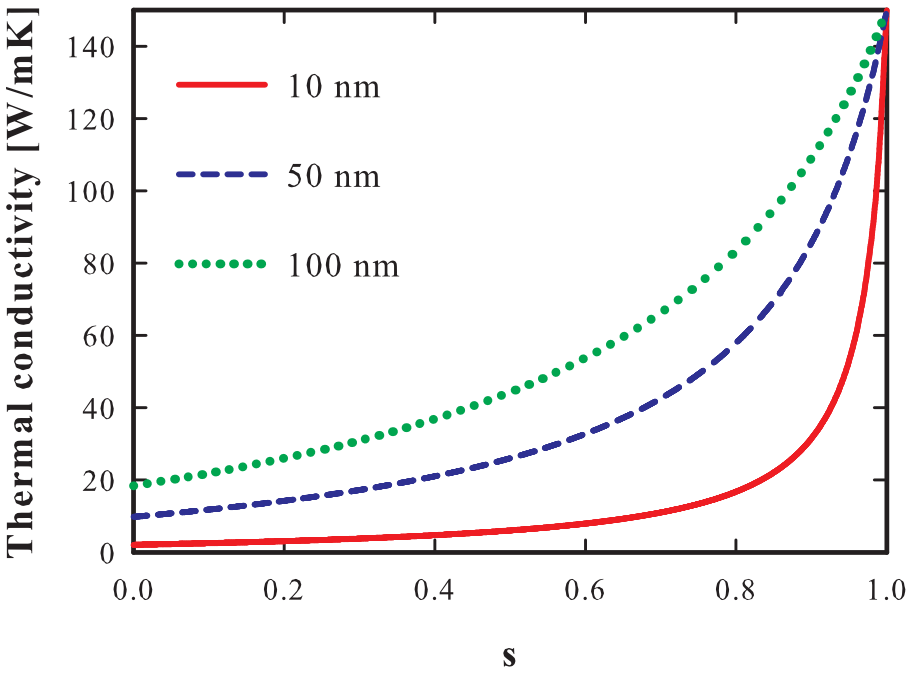

Figure 4.3: Interfacial specularity dependency of the thermal conductivity of suspended particles in different particle sizes.

Figure (4.4) shows the effective thermal conductivity of an inhomogeneous media with spherical particles as a function of the volume fraction for three different particle sizes. Results are presented for a $SiGe$ nanocomposite with Si particles suspended in a Ge matrix. This nanocomposite has also been previously simulated by the Monte Carlo method. The parameters required in the calculation are presented in Table (4.1).
Bulk mean free paths of epoxy and aluminum nitride (AlN) are calculated from $\Lambda_b = 3k/Cv$ by considering thermal conductivities of epoxy and AlN are 0.168 [49] and 320 [50] $Wm^{-1}K^{-1}$, respectively. The unmodified Hashin's model (equation (2.107)) is in

Table 4.1: Material parameters used in calculations.

Material	Specific Heat $[\times 10^6 Jm^{-3}K^{-1}]$	Group Velocity $[ms^{-1}]$	Bulk Mean Free Path $[nm]$	Density $[kgm^{-3}]$
Si (Ref. [17])	0.93	1804	268	2330
Ge (Ref. [17])	0.87	1042	171	5330
SiO_2 (Ref. [16])	1.687	4400	0.558	2278
AlN (Ref. [50])	2.7	6972	51	3300
$Epoxy$ (Ref. [51])	1.91	2400	0.11	1970

extremely poor agreement with the Monte Carlo simulation results, which is expected since the corresponding bulk thermal conductivities of the matrix and suspended particles are used to determine the effective thermal conductivity of the nanocomposite. On the other hand, the internal thermal resistances in the matrix and nanoparticles are more significant than the influence of the boundary scattering, since the perfect interface (no thermal boundary resistance) between the matrix and suspended particles are assumed in Hashin's model. It is important to point out that the influence of the particle size is not considered in this model. Our diffuse (i.e., $s = 0$) effective thermal conductivity

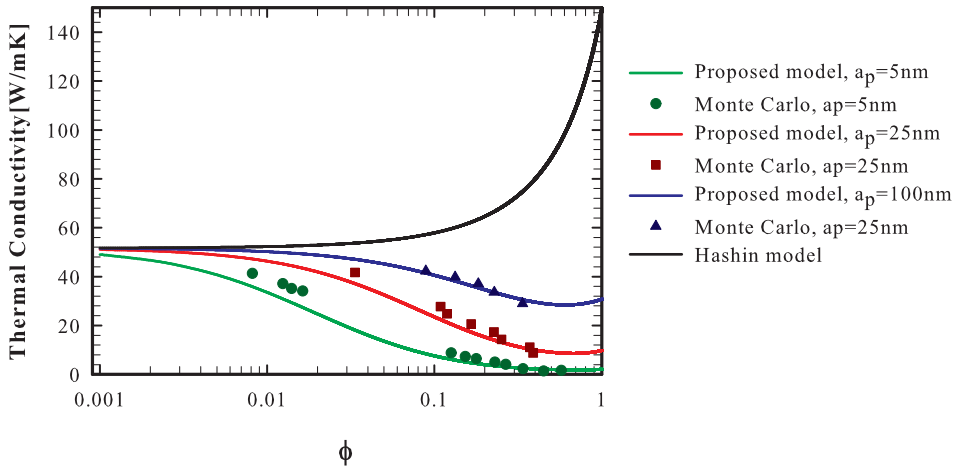

Figure 4.4: Thermal conductivity of a *SiGe* nanocomposite as a function of the particle diameter and the volume fraction. Proposed model is compared with Hashin's model and obtained results from Monte Carlo simulations.

is compared to Nan's model for three particle sizes (see Figure (4.5)). Although, Nan's model represents a better approximation than Hashin's model, this model is not still able to estimate precisely the effective thermal conductivity of nanocomposite, especially at smaller particle sizes where the effect of the interface scattering due to the particle size is undeniable. When compared to Hashin's model, Nan's model has a term to introduce the particle size effect on the effective thermal conductivity of the inhomogeneous media. Indeed, the particle size dependence of the effective thermal conductivity is presented by the traditional dimensionless thermal boundary resistance term (i.e. α).

Figure (4.6) compares results of our model with the Minnich-Chen model and Monte Carlo simulations for a_p =5, 25, 100 nm. In the case $s = 1$ (i.e., for pure specular reflection) the agreement is poor. On the other hand, the effective thermal conductivity with diffuse reflection (i.e., the case when $s = 0$) agrees well with Monte Carlo simulations

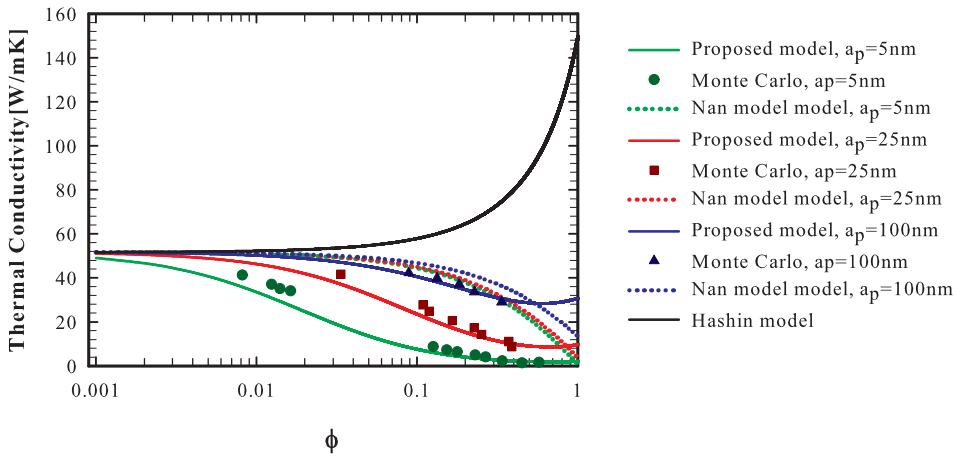

Figure 4.5: Thermal conductivity of a *SiGe* nanocomposite as a function of the particle diameter and the volume fraction. Proposed model is compared with Hashin's model, Nan's model and obtained results from Monte Carlo simulations.

for all volume fractions. A significant difference between the specular and diffuse effective thermal conductivities is observed for higher volume fractions. It is worthwhile to note that our results (except $s = 1$) are similar to those presented by Minnich and Chen for smaller particle volume fractions. For all particle sizes, the proposed formula for diffuse (i.e., $s = 0$) effective thermal conductivity predicts higher values than the Minnich-Chen formula and approaches the effective thermal conductivity of suspended nanoparticles when $\phi \to 1$. This difference becomes significant with an increase in the particle radius. Our results still differ from those presented by Minnich-Chen model for smaller particle sizes in moderate volume fractions. Using an appropriate value of s, our results are in the good agreement with the Monte Carlo simulation for all particle sizes. Our results also indicate how the effective thermal conductivity of the nanocomposite would change if the particle-matrix surfaces were modified (for example lowering temperature to a few Kelvin or changing the roughness of the nanoparticle) to favor specular reflections.

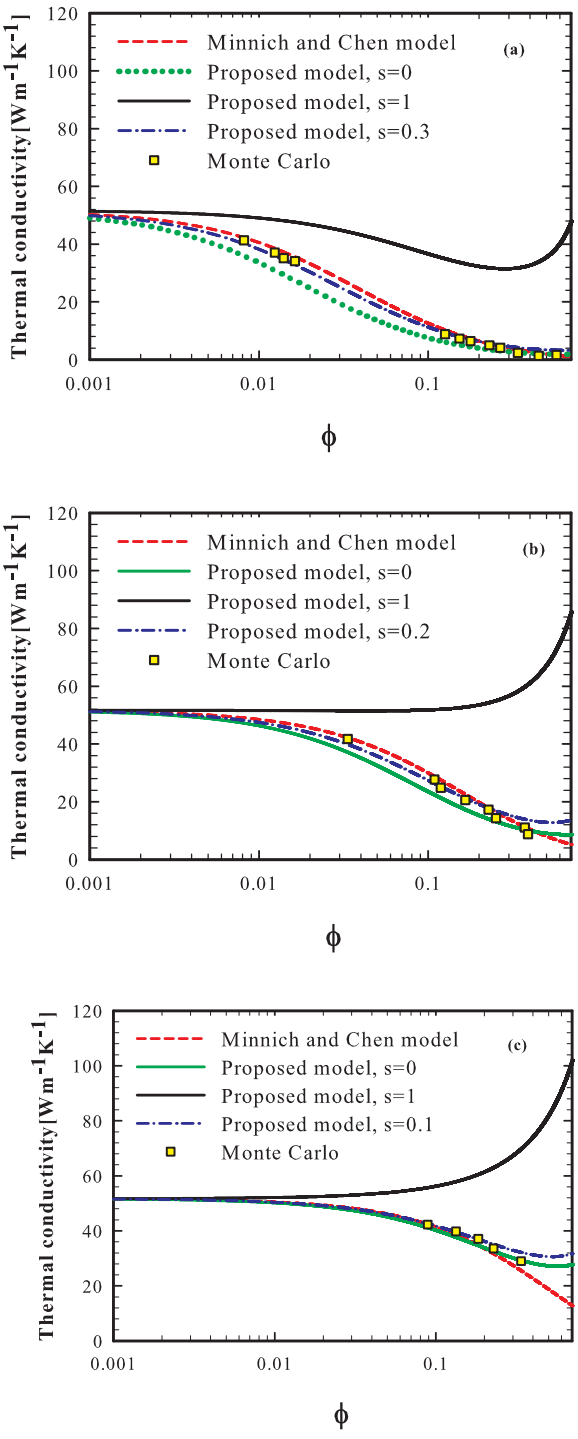

Figure 4.6: Effective thermal conductivity of a SiGe nanocomposite comprising spherical Si particles with the radius: (a) $a_p = 5nm$, (b) $a_p = 25nm$ and (c) $a_p = 100nm$ as a function of the particle volume fraction ϕ.

Plotted in Figure (4.7) for a nanocomposite with suspended SiO_2 particles, our re-

sult is in excellent agreement with experimental data, while our model underpredicts the thermal conductivity of a nanocomposite with AlN particles. Recently reported experimental results [49] show that AlN nanoparticles have different shapes: cubic, spherical and hexagonal with a wide particle size distribution, while SiO_2 nanoparticles are spherical and show a narrow particle size distribution. Since in the derivation of our model uniform particle size distribution and quite spherical shape of nanoparticles are assumed, our analytical results are in better agreement with SiO_2 than AlN.

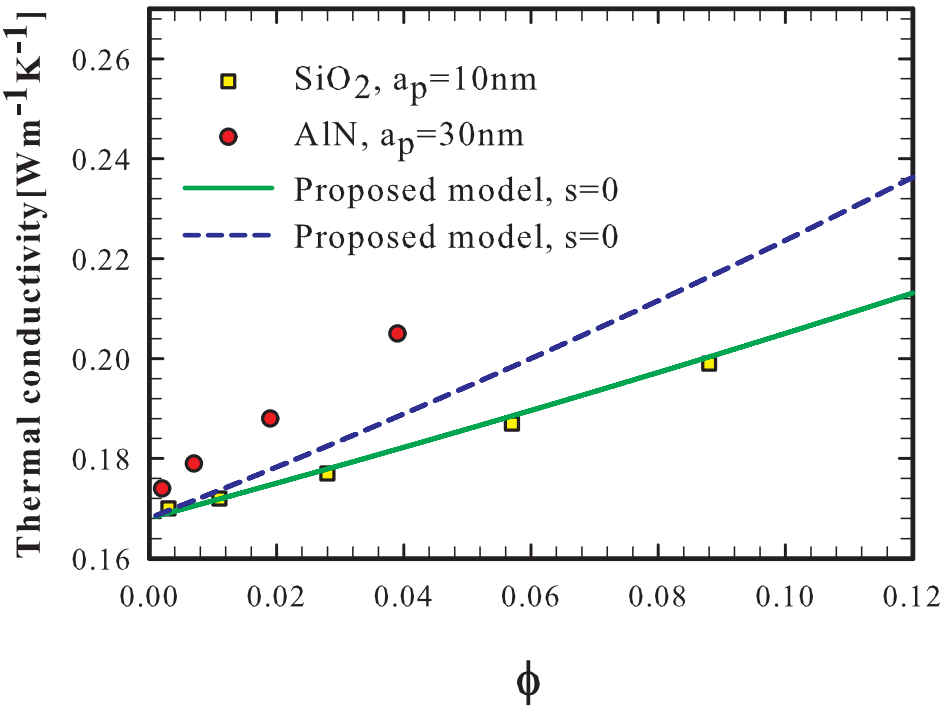

Figure 4.7: Experimental and calculated values of the effective thermal conductivity as a function of the volume fractions ϕ of SiO_2 and AlN embedded in epoxy resin.

Chapter 5

Conclusion

5.1 Conclusion

In this dissertation, heat transfer in a heterogeneous media comprising suspended spherical particles has been studied. This work is motivated by understanding phonon transport at the interface between dissimilar materials. In particular, a new generic formula for the effective thermal conductivity coefficient is proposed, which is a multi-scale formula with the ability to predict the effective thermal conductivity in a wide range of particle sizes and volume fractions. The effective mean free path is used to study the behaviour of phonons at boundaries. A new thermal boundary resistance mean free path term is proposed to take the reflection and transmission of phonons at the interface between particle and matrix into account. The specular and diffuse scatterings of phonons at the particle-matrix interface are investigated. Results show that the effective thermal conductivity of the nanocomposite increases with increasing particle size due to a reduction in the effective area for phonon-particle collisions. On the other hand, the interfacial scattering effects are neglected for higher particle sizes. Our results are compared with results from Monte Carlo simulations and reported experimental data. There is good agreement between our results and Monte Carlo simulation results. Our results agree well with experimental data when suspended particles are assumed spherical with a narrow particle size distribution.

5.2 Recommendation for future works

The following unexplored topics are recommended for future research:
(i). Frequency-dependent properties, such as a frequency-dependent mean free path, can be incorporated into the generic formula. One needs only to consider the frequency-dependent effective mean free path, specific heat and velocity of each phase.
(ii). Study of heat transport in a heterogeneous media composed of thin films in a matrix. The effective thermal conductivity of the nanocomposite can be investigated in both longitudinal and transverse directions. The effects of orientation of thin films and particle size distribution on the effective thermal conductivity can be studied as well.
(iii). Investigation of the phonon transport at the nanowire-matrix interface and presentation a new generic formula for the effective thermal conductivity of nanocomposites with nanowires suspended in a matrix. Effect of orientation, size, phonon transport mechanisms (specular or diffuse) on the effective thermal conductivity can be considered.

Chapter 6

Bibliography

[1] G. Chen, "Particularities of heat conduction in nanostructures," *Journal of Nanoparticle Research*, vol. 2, pp. 199–204, 2000.

[2] M. E. Siemens, Q. Li, R. Yang, K. A. Nelson, E. H. Anderson, M. M. Murnane, and H. C. Kapteyn, "Quasi-ballistic thermal transport from nanoscale interfaces observed using ultrafast coherent soft x-ray beams," *Nature Materials*, vol. 9, no. 1, pp. 26–30, 2010.

[3] G. Lebon D. Jou, *Extended Irreversible Thermodynamics,*, Springer, New York, 2010.

[4] G. Chen, *Nanoscale Energy Transport and Conversion: A Parallel Treatment of Electrons, Molecules, Phonons, and Photons*, Oxford University Press, USA, 2005.

[5] C. V. D. R. Anderson and K. K. Tamma, "An overview of advances in heat conduction models and approaches for prediction of thermal conductivity in thin dielectric films," *International Journal of Numerical Methods for Heat and Fluid Flow*, vol. 14, no. 1, pp. 12–65, 2004.

[6] J. E. Turney, A. J. H. McGaughey, and C. H. Amon, "In-plane phonon transport in thin films," *Journal of Applied Physics*, vol. 107, no. 2, pp. 024317, 2010.

[7] D. P. Sellan, J. E. Turney, A. J. H. McGaughey, and C. H. Amon, "Cross-plane phonon transport in thin films," *Journal of Applied Physics*, vol. 108, no. 11, pp. 113524, 2010.

[8] T. M. Tritt, *Thermal Conductivity, Theory, Properties and Applications.*, Kluwer Academic/Plenum Publishers, New York, 2004.

[9] C. Kittel, *Introduction to Solid State Physics*, Wiley New Jersey, 2005.

[10] J. Angus D. Howard, *Acoustics and Psychoacoustics*, Elsevier Ltd. , USA, 2009.

[11] Z. M. Zhang, *Nano/Microscale Heat Transfer*, McGraw-Hill, 2009.

[12] A. A. Joshi and A. Majumdar, "Transient ballistic and diffusive phonon heat transport in thin films," *Journal of Applied Physics*, vol. 74, no. 1, pp. 31–39, 1993.

[13] C. V. D. R. Anderson and K. K. Tamma, "Novel heat conduction model for bridging different space and time scales," *Physical Review Letters*, vol. 96, pp. 184301, May 2006.

[14] M. Asheghi, K. Kurabayashi, R. Kasnavi, and K. E. Goodson, "Thermal conduction in doped single-crystal silicon films," *Journal of Applied Physics*, vol. 91, no. 8, pp. 5079–5088, 2002.

[15] G. Chen, "Ballistic-diffusive heat-conduction equations," *Physical Review Letters*, vol. 86, pp. 2297–2300, Mar 2001.

[16] T. Zeng and G. Chen, "Phonon heat conduction in thin films: Impacts of thermal boundary resistance and internal heat generation," *Journal of Heat Transfer*, vol. 123, no. 2, pp. 340–347, 2001.

[17] G. Chen, "Thermal conductivity and ballistic-phonon transport in the cross-plane direction of superlattices," *Phys. Rev. B*, vol. 57, pp. 14958–14973, 1998.

[18] R. Yang, G. Chen, and M. S. Dresselhaus, "Thermal conductivity of simple and tubular nanowire composites in the longitudinal direction," *Phys. Rev. B*, vol. 72, pp. 125418, 2005.

[19] A. Majumdar, "Microscale heat conduction in dielectric thin films," vol. 115, no. 1, pp. 7–16, 1993.

[20] E. S. Landry and A. J. H. McGaughey, "Thermal boundary resistance predictions from molecular dynamics simulations and theoretical calculations," *Physical Review B*, vol. 80, no. 16, 2009.

[21] P. J. Antaki, "Importance of nonFourier Heat Conduction in Solid-Phase Reactions," *Combustion and Flame*, vol. 112, no. 3, pp. 329–341, 1998.

[22] K. Razi Naqvi and S. Waldenstrom, "Brownian motion description of heat conduction by phonons," *Phys. Rev. Lett.*, vol. 95, pp. 065901, 2005.

[23] P. M. Norris, J. L. Smoyer, J. C. Duda, and P. E. Hopkins, "Prediction and Measurement of Thermal Transport Across Interfaces Between Isotropic Solids and Graphitic Materials," *Journal of Heat Transfer*, vol. 134, no. 2, 2012.

[24] E. T. Swartz and R. O Pohl, "Thermal-Boundary Resistance," *Reviews of Modern Physics*, vol. 61, no. 3, pp. 605–668, JUL 1989.

[25] G. C. Loh, B. K. Tay, and E. H. T. Teo, "Flux-mediated diffuse mismatch model," *Applied Physics Letters*, vol. 97, no. 12, pp. 121917, 2010.

[26] P. E. Hopkins and P. M. Norris, "Relative contributions of inelastic and elastic diffuse phonon scattering to thermal boundary conductance across solid interfaces," *Journal of Heat Transfer*, vol. 131, no. 2, pp. 1–9, 2009.

[27] P. E. Hopkins, "Multiple phonon processes contributing to inelastic scattering during thermal boundaryconductance at solid interfaces," *Journal of Applied Physics*, vol. 106, no. 1, pp. 013528, 2009.

[28] W. A. Little, "The transport of heat between dissimilar solids at low temperatures," *Canadian Journal of Physics*, vol. 37, no. 3, pp. 334–349, 1959.

[29] M. Szymaski, "Calculation of the cross-plane thermal conductivity of a quantum cascade laser active region," *Journal of Physics D: Applied Physics*, vol. 44, 2011.

[30] D. P. H. Hasselman and L. F. Johnson, "Effective thermal conductivity of composites with interfacial thermal barrier resistance," vol. 21, no. 6, pp. 508–515, 1987.

[31] Y. Benveniste, "Effective thermal conductivity of composites with a thermal contact resistance between the constituents: Nondilute case," *Journal of Applied Physics*, vol. 61, no. 8, pp. 2840–2843, 1987.

[32] C.-Wen Nan, R. Birringer, D. R. Clarke, and H. Gleiter, "Effective thermal conductivity of particulate composites with interfacial thermal resistance," *Journal of Applied Physics*, vol. 81, no. 10, pp. 6692–6699, 1997.

[33] A. J. Minnich and G. Chen, "Modified effective medium formulation for the thermal conductivity of nanocomposites," *Applied Physics Letters*, vol. 91, no. 7, pp. 073105, 2007.

[34] J. Ordonez-Miranda, R. Yang, and J. J. Alvarado-Gil, "On the thermal conductivity of particulate nanocomposites," *Applied Physics Letters*, vol. 98, no. 23, pp. 233111, 2011.

[35] C. Dames and G. Chen, "Theoretical phonon thermal conductivity of si/ge superlattice nanowires," *Journal of Applied Physics*, vol. 95, no. 2, pp. 682–693, 2004.

[36] A. L. Moore, S. K. Saha, R. S. Prasher, and L. Shi, "Phonon backscattering and thermal conductivity suppression in sawtooth nanowires," *Applied Physics Letters*, vol. 93, no. 8, pp. 083112, 2008.

[37] Z. Ge, D. G. Cahill, and P. V. Braun, "Thermal conductance of hydrophilic and hydrophobic interfaces," *Phys. Rev. Lett.*, vol. 96, pp. 186101, 2006.

[38] J. Ordonez-Miranda and J. J. Alvarado-Gil, "Thermal conductivity of nanocomposites with high volume fractions of particles," .

[39] G. Chen, "Nonlocal and nonequilibrium heat conduction in the vicinity of nanoparticles," *Journal of Heat Transfer*, vol. 118, no. 3, pp. 539–545, 1996.

[40] E. H. Sondheimer, "The mean free path of electrons in metals," *Advances in Physics*, vol. 50, no. 6, pp. 499–537, 2001.

[41] A. Nabovati, D. P. Sellan, and C. H. Amon, "On the lattice Boltzmann method for phonon transport," *Journal of Computational Physics*, vol. 230, no. 15, pp. 5864–5876, 2011.

[42] G. H. Tang, Y. Zhao, G. X. Zhai, and C. Bi, "Phonon boundary scattering effect on thermal conductivity of thin films," *Journal of Applied Physics*, vol. 110, no. 4, 2011.

[43] M. I. Flik and C. L. Tien, "Size effect on the thermal conductivity of thin-film superconductors," *Journal of Heat Transfer*, vol. 112, no. 4, pp. 872–881, 1990.

[44] Ziman J. M., *Electrons and Phonons: The Theory of Transport Phenomena in Solids*, Clarendon, Oxford, 1960.

[45] Y. S. Ju and K. E. Goodson, "Phonon scattering in silicon films with thickness of order 100 nm," *Applied Physics Letters*, vol. 74, no. 20, pp. 3005–3007, 1999.

[46] W. Liu and M. Asheghi, "Phonon-boundary scattering in ultrathin single-crystal silicon layers," *Applied Physics Letters*, vol. 84, no. 19, pp. 3819–3821, 2004.

[47] M. Asheghi, M. N. Touzelbaev, K. E. Goodson, Y. K. Leung, and S. S. Wong, "Temperature-dependent thermal conductivity of single-crystal silicon layers in soi substrates," *Journal of Heat Transfer*, vol. 120, pp. 30–36, 1998.

[48] F. Yang, T. Ikeda, G. J. Snyder, and C. Dames, "Effective thermal conductivity of polycrystalline materials with randomly oriented superlattice grains," *Journal of Applied Physics*, vol. 108, no. 3, pp. 034310, 2010.

[49] R. Kochetov, A. V. Korobko, T. Andritsch, P. H. F. Morshuis, S. J. Picken, and J. J. Smit, "Modelling of the thermal conductivity in polymer nanocomposites and the impact of the interface between filler and matrix," *Journal of Physics D: Applied Physics*, vol. 44, no. 39, pp. 395401, 2011.

[50] Y. Zhao, C. Zhu, S. Wang, J. Z. Tian, D. J. Yang, C. K. Chen, H. Cheng, and P. Hing, "Pulsed photothermal reflectance measurement of the thermal conductivity of sputtered aluminum nitride thin films," *Journal of Applied Physics*, vol. 96, no. 8, pp. 4563–4568, 2004.

[51] H. M. Duong, N. Yamamoto, K. Bui, D. V. Papavassiliou, S. Maruyama, and B. L. Wardle, "Morphology effects on nonisotropic thermal conduction of aligned single-walled and multi-walled carbon nanotubes in polymer nanocomposites," *The Journal of Physical Chemistry C*, vol. 114, no. 19, pp. 8851–8860, 2010.